DESIGN OF PASSIVE DECAY HEAT REMOVAL SYSTEM FOR THE LEAD COOLED FLEXIBLE CONVERSION RATIO FAST REACTOR

By

Joshua Whitman

SUBMITTED TO THE DEPARTMENT OF NUCLEAR SCIENCE AND ENGINEERING IN PARTIAL FULFILLMENT OF THE REQUIREMENTS FOR THE DEGREE OF

BACHELOR OF SCIENCE IN NUCLEAR SCIENCE AND ENGINEERING
AT THE
MASSACHUSETTS INSTITUTE OF TECHNOLOGY

June 2007

Signature of Author: _____
Joshua J. Whitman
Department of Nuclear Science and Engineering
5/21/07

Certified by: _____
Neil E. Todreas
Professor of Nuclear Science and Engineering (Emeritus)
Thesis Supervisor

Accepted by: _____
David G. Cory
Professor of Nuclear Science and Engineering
Chairman, NSE Committee for Undergraduate Students

DESIGN OF PASSIVE DECAY HEAT REMOVAL SYSTEM FOR THE LEAD COOLED FLEXIBLE CONVERSION RATIO FAST REACTOR

By

Joshua Whitman

Submitted to the Department of Nuclear Science and Engineering on 5/21/07
In Partial Fulfillment of the Requirements for the Degree of
Bachelor of Science in Nuclear Science and Engineering

ABSTRACT

The lead-cooled flexible conversion ratio fast reactor shows many benefits over other fast-reactor designs; however, the higher power rating and denser primary coolant present difficulties for the design of a passive decay heat removal system. In order to achieve passive cooling, enhancements are needed over current designs, such as the S-PRISM and ABR, which utilize passive cooling through the reactor vessel to atmospheric air. Enhancements such as axial fins, a perforated plate, and round indentations, or dimples, were considered as additions to the hot air riser to increase heat transfer. Other enhancements include a liquid metal bond between the reactor and guard vessels, and a dual-level design which introduces ambient temperature air halfway up the vessel wall. A code was written in Java to simulate these conditions, leading to a promising case using dimples on the guard vessel wall as the primary mode of heat transfer enhancement, and including the dual-level design. A conservative estimate of dimple performance indicates that during a passive decay heat removal shutdown, bulk primary coolant temperature will peak at 713 °C, giving a 12 °C margin to clad failure. Attempts were made to refine the uncertainty within the calculations using a computational fluid dynamics code, Fluent, but these ultimately were unsuccessful.

Additional studies were conducted on the static stress imparted on the vessel, and the dynamic stress caused by a seismic event. The static stress was found to be within ASME code limits. Seismic analysis determined that a seismic isolation scheme would be necessary in order to prevent damage to the vessel during an earthquake.

Thesis Supervisor: Neil E. Todreas
Title: Professor of Nuclear Science and Engineering (Emeritus)

Acknowledgements

I would like to express my gratitude for the guidance and assistance provided by my thesis advisor, Professor Neil Todreas. I would also like to extend special thanks to Dr. Pavel Hejzlar for his patience, time, and support throughout this project. Finally, additional thanks are put forth to Dr. Lin-wen Hu and Antoine Chupin for their assistance with Fluent, and Professor Jacopo Buongiorno for his help with this study.

1. Introduction

1.1. Overview of FCR Reactor Goals

Current nuclear power plants use only a small fraction of the energy stored in mined uranium. While nuclear fuel is currently abundant and cheap, in the future it is anticipated that world uranium supplies will decrease and cause nuclear fuel costs to increase. Additionally, the cost of nuclear waste disposal is a concern. Currently the United States plans to bury its waste in the planned Yucca Mountain repository; however, the project has been stalled for some time pending lawsuit resolution and certification by the EPA and NRC. The problems of fuel supply and waste disposal will need to be overcome in the near future if nuclear power is going to succeed in increasing its global presence.

The Flexible Conversion Ratio (FCR) Fast Reactor aims to solve both of these problems. A plant with conversion ratio (CR) 1, also known as a converter, acts as a self-sustaining reactor where all actinides are recycled into the core until they are fissioned. This both minimizes waste and maximizes the total power captured from the natural uranium. Alternatively, a plant with conversion ratio 0, a burner, will fission and transmute the longer-lived radionuclides which contribute the bulk of the dose from spent light water reactor (LWR) waste. With the ability to swap a core optimized for converting with one optimized for burning, the FCR reactor will have the flexibility to fit whichever task is needed. This will also reduce the capital risk in building such a plant, as it could potentially act as a burner until all of the LWR waste is used up, and then switch to unity conversion ratio instead of needing to be decommissioned or going into part-time use.

The US Department of Energy is currently working to identify a design that meets the flexible conversion ratio requirement and other criteria such as safety and cost. Much work has been done on both gas and sodium cooled designs by MIT and ANL, respectively. These designs, while promising, have drawbacks as well. Gas cooled reactors have difficulty achieving passive safety, and sodium coolant reacts exothermically with water and oxygen. Thus the purpose of this project is to investigate the feasibility of designing a reactor that will use liquid lead as its primary coolant. Final designs will be evaluated based on preset criteria, including core flexibility, safety, and cost concerns.

Nuclear plants currently in operation rely on "active" decay heat removal systems, where pumps force coolant through the core and heat exchangers to maintain proper core temperature after the reactor shuts down. More recent theoretical designs, on the other hand, have relied heavily on "passive" safety systems, where natural circulation of the primary coolant results in the desired heat transfer effects. Advantages of such a system include ability to safely cool the core in the absence of electricity, increased reliability, and general simplification and cost reduction as a result of removing excess machinery and coolant loops. As the currently presented sodium design includes passive safety systems, this will be a necessity for the lead cooled design if it is to be competitive.

While in many ways the decay heat removal approach for a lead cooled reactor is similar to that of sodium, two differences greatly increase the difficulty in successfully designing a DHR system for the FCR reactor. First, the power rating of the reactor is increased above that of the leading sodium designs by a factor of 2.4. This is due to the belief that, in order to be economically competitive with LWRs and maximize economies of scale, a fast reactor must produce around 1000 MW of electricity. An addition concern specific to lead is that the higher density of the coolant necessitates a thicker supporting vessel. This directly increases the thermal resistance between the core and the heat sink during a loss of forced flow accident, decreasing the ability to passively cool the core.

1.2. Overview of Reactor Design

The lead cooled FCR reactor has a design similar to other pool-type fast reactors such as the Korean Lead-cooled Fast Reactor (KLFR) and General Electric's (GE's) Super-Power Reactor Innovative Small Module (S-PRISM). The design uses a single vessel to completely contain the primary coolant system. The use of liquid metals allows the primary side to operate at atmospheric pressures, which when coupled with a lack of primary coolant paths outside of the vessel eliminates the risk of a loss of coolant accident.

The lead-cooled FCR reactor has a 2400 MWth core power rating and uses a high-efficiency Supercritical CO_2 cycle (S-CO_2) to achieve a power rating near 1000 MWe. This power was chosen in order to increase economic competitiveness while still attempting to keep the reactor as modular as possible. By using liquid lead as the primary coolant, the reactor avoids the need for a high-pressure reactor vessel as is the case with current operating LWRs.

Other liquid metals that have been proposed for such applications are liquid sodium and a lead-bismuth eutectic. Sodium reacts exothermically with water and oxygen, which can severely complicate the necessary reaction to a primary coolant leak; however sodium does have superior thermal and heat transfer qualities, and is less dense than water, which greatly alleviates vessel strength issues for both static stress analysis, and potential damage from seismic events. Lead-bismuth eutectic has similar qualities to lead, but with a lower melting point, but bismuth is not a commonly available metal, and so there are significant issues over potential cost and supply chain issues. Additionally, ^{209}Bi is activated by a neutron flux to become ^{210}Po, a toxic alpha emitter with half life of about 140 days. While this reaction still occurs in a lead-cooled reactor, it is on a much smaller scale [Hejzlar et al., 2004]. Thus it is desired to design a reactor the uses lead as a primary coolant.

Within the reactor vessel the primary coolant flows in a dual-free level path as shown in Figure 1.1. The liquid lead flows up through the core and chimney, down through the

supercritical CO_2 heat exchangers, up through the vessel liner, and then back down through the primary coolant pumps. This design prevents the CO_2 from being blown down and into the core causing voiding in the event of a heat exchanger tube rupture.

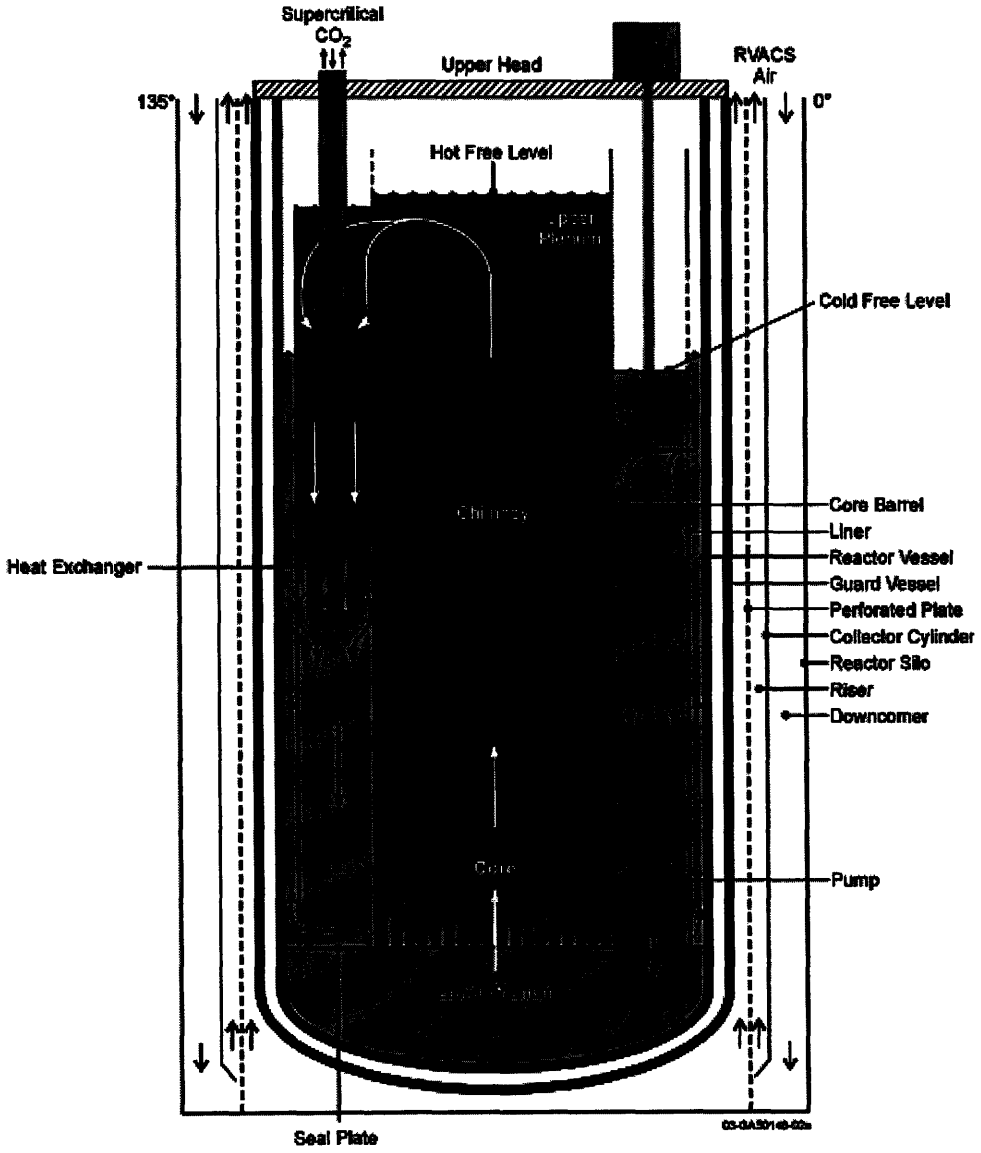

Figure 1.1 Schematic of reactor vessel with dual-free level [from Hejzlar et al., 2004]

It is desired to keep the primary heat exchangers completely within the reactor vessel for cost, simplicity, and safety considerations. Avoiding the need for an intermediate loop reduces complexity while increasing thermal efficiency of the cycle, and eliminates the need for removing the primary coolant from within the reactor vessel to an external heat exchanger, as this increases the possibility of a loss of coolant accident.

1.3. Thesis Objectives

The primary objective of this thesis is to design an acceptable passive decay heat removal system for the 2400 MWth lead-cooled FCR reactor. This will require quantitative analysis of different DHR schemes using various computer codes. These codes will perform such tasks as determining bulk heat transfer from the vessel to the atmosphere, determining primary coolant temperature during a passive decay heat removal event, and determining the temperature of important structural components for stress analysis during shutdown. Ultimately the goal is to create a design that will remove the decay heat from a vessel in the event of a loss of offsite power without exceeding key clad, fuel, or vessel temperature limits. The design must also take into account the dynamic stress placed on the vessel during a seismic event, and should be able to withstand multiple passive DHR shutdown events without exceeding ASME limits for loading at high temperatures. Additionally, goals for the design are simplicity of design and reduced construction and maintenance costs.

2. Literature Review of Passive Safety Systems

2.1. Westinghouse AP1000

The reactor that is most likely to be built in the near future that incorporates passive safety is the Westinghouse-designed AP-1000. This pressurized water reactor (PWR) with a power rating of about 1000 MWe is designed with the intent of simplifying and improving upon current PWR designs while incorporating passive safety. During a loss of offsite power, the reactor uses a series of "fail-safe" valves to open a coolant path for the reactor water through a passive residual heat removal heat exchanger located within a pool of water kept inside containment, called the in-containment refueling water storage tank (IRWST). This pool will heat up and eventually boil, whereupon the water vapor will contact the cool containment wall, condense, and drip back into the IRWST. This loop is illustrated in Figure 2.1. While the containment is capable of maintaining this cooler temperature through natural convection with the ambient air, there is also a water tank located on top of the containment that can be released to help cool the outer surface of the containment, giving a greater margin to failure of the containment vessel. The containment vessel has a diameter 36.9m, and a height around 30 m [Cummins et al. 2003]. This provides a very large surface area for heat transfer as compared to many of the fast reactor designs, including those discussed below. Additionally, parts of this system are integrated into another system to flood the core with water from the IRWST during a loss of coolant accident; however, since the FCR has a low-pressure reactor vessel and guard vessel without any external piping of the primary coolant, this is not an important feature to consider for the design presented in this thesis.

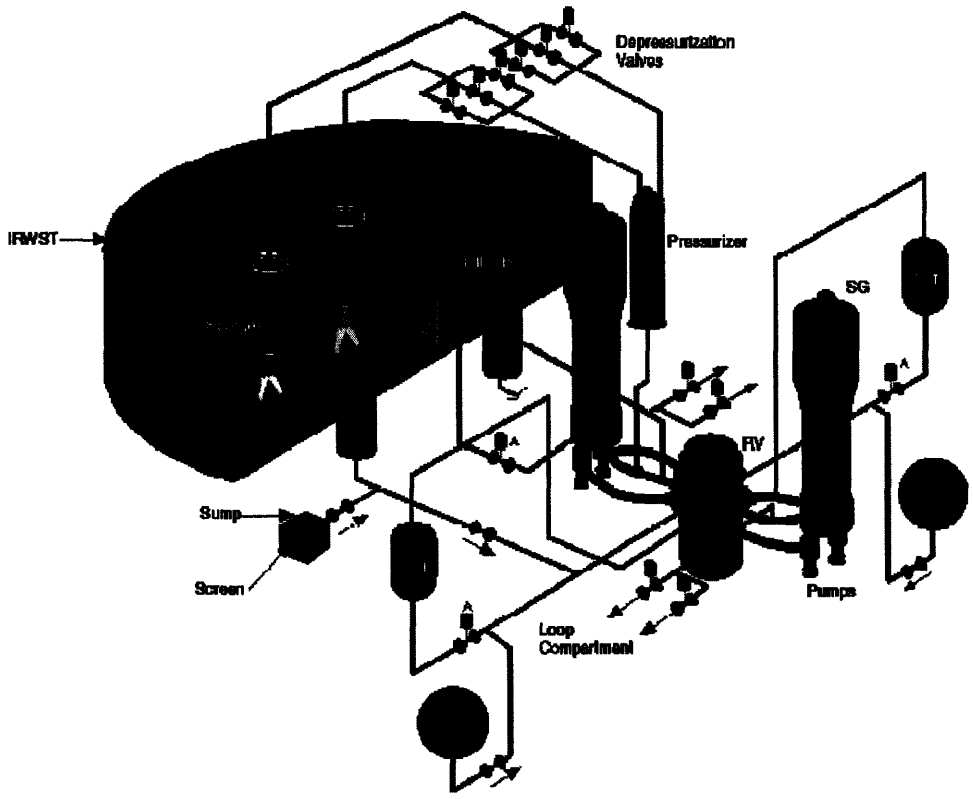

Figure 2.1. AP1000 Reactor Coolant System and Passive Core Cooling System. From Cummins et al. [2003].

2.2. General Electric S-PRISM

The S-PRISM is a 1000MWth sodium-cooled fast reactor designed by General Electric. This reactor is designed to be modular, meaning that it would be possible to construct the reactor components, including the containment vessel, in a factory and ship the modules by barge to be assembled in the reactor's final location. The primary coolant loop is contained entirely within the 5cm thick reactor vessel, which is nested within the 2.5 cm thick guard vessel. This outer vessel, which also serves as the reactor's containment, stands roughly 20m tall and 10m in diameter. Between the two vessels a 20cm gap is filled with argon gas. It is through these two vessels that the decay heat is removed in the event that the intermediate sodium loop and offsite power are both compromised.

The passive decay heat removal strategy for the SPRISM is made up of two separate and complementary systems, the RVACS and the Auxiliary Cooling System, or ACS. Both utilize natural circulation of atmospheric air driven by buoyancy and share air inlets and chimneys. The ACS uses the intermediate heat transport system to supplement the RVACS. When operational, natural circulation within the primary and intermediate coolant loops transfers heat to the air riser, where the air flowing past serves as the final heat sink. The RVACS operates by removing heat through the walls of the reactor and guard vessels in a similar fashion. Heat is again transferred within the primary loop through natural circulation. Since the primary coolant cannot be piped outside of the containment vessel the performance of the RVACS is constrained primarily by the surface area of this vessel. GE was able to increase the performance of the RVACS system by adding a perforated collector cylinder, or plate, to the hot air riser. [Boardman et al. 2000] The perforated plate and the solid collector cylinder wall are both heated through radiation heat transfer, and the heat is then convected from four surfaces (guard vessel outer wall, collector cylinder inner wall, and two sides of the perforated plate), rather than just two. This enhancement is discussed further in Section 3.4. This advance allowed GE to increase the power rating of the S-PRISM to 1000MWth per module over the 840 MWth Advanced Liquid Metal Reactor, or ALMR, which the design was extensively modeled after.

2.3. ABR/MABR/ABRT

The FCR reactor can be described as a scaled-up version of the fertile-free Actinide Burner Reactor (ABR), the fertile-free Minor Actinide Burner Reactor (MABR), and the Actinide Burner Reactor with Thorium (ABRT), which all share the same thermal properties and differ only in core configuration and number of control rods. These reactors share designs for reactor vessel, heat exchangers, Balance of Plant, and passive DHR. They are all lead-cooled, and are rated as 700MWth, 300MWe [Todreas et al. 2004].

The design is similar to the S-PRISM in that the primary coolant is contained entirely within the reactor vessel, and DHR is performed by a RVACS unit using a perforated

plate for enhanced heat transfer. As one of the goals of the design is increased modularity, the vessel size is considerably smaller than the S-PRISM at 6.34m in diameter and 19m tall. This decreased size allows for transport of the vessel on a special limited-access rail car from the factory to the assembly site.

Because the ABR, MABR, and ABRT design does not include any seismic isolation, a 25cm thick guard vessel was chosen to withstand the weight of the coolant during and earthquake. This caused a steep drop in the DHR rates and necessitated the addition of a liquid metal bond between the reactor vessel and the guard vessel. This is adopted in the FCR design as well.

2.4. KLFR

Another lead-cooled design closely related to the FCR project in design is the Korean Lead-cooled Fast Reactor, or KLFR. The KLFR is designed with a power rating of 900 MWth, 372 MWe, and also uses a modified RVACS design for decay heat removal. Similar to the S-PRISM, the containment vessel has a diameter of around 9m, and uses radiation structures in the air riser. The radiation structures are situated horizontally across the riser, unlike the S-PRISM's vertical perforated plate. Additionally, the KLFR utilized a liquid lead bond in the gap between the reactor and containment vessel.

While the DHR system for the KLFR is similar to that for the FCR, some of the final design decisions are questionable. In the analysis provided by Eoh et al. [2005], the metal bond between the reactor and guard vessel is considered to be liquid, and convection currents are included in the heat transfer calculation; however, lead is solid at the normal operating temperature of the reactor, and would therefore take some time to melt before this mode of heat transfer could be considered. Additionally, the phase-change may cause adverse effects in the form of putting stress on one or both of the vessels that it touches. Without further research into the consequences of this, liquid lead appears to be a poor choice for this task.

Another questionable design in the KLFR decay heat removal system is the radiation structures, depicted in Figure 2.2. These are poorly explained in the literature, and some of the conclusions drawn seem highly counterintuitive. One graph, shown in Figure 2.3, appears to show that the heat removal rate for an RVACS without radiation structures is independent of the riser width. This can be seen by comparing the left-most points. This can easily be proven to be false. Additionally, a performance saturation point is seen when the number of radiation structures is increased, whereas a peak and subsequent decrease in decay heat removal would be expected, as the radiation effects saturate but the pressure drop continues to increase. This is never explained in the text.

Finally, the description of the radiation structures is confusing and vague. For these reasons the structures presented were not included in the analysis completed for this thesis.

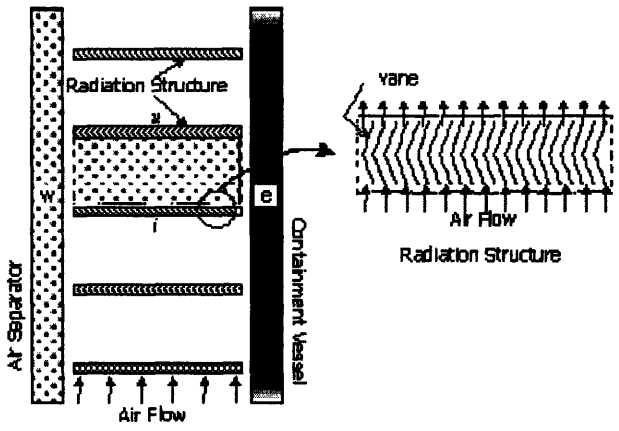

Figure 2.2. KLFR radiation structure layout. From Eoh et al. [2005].

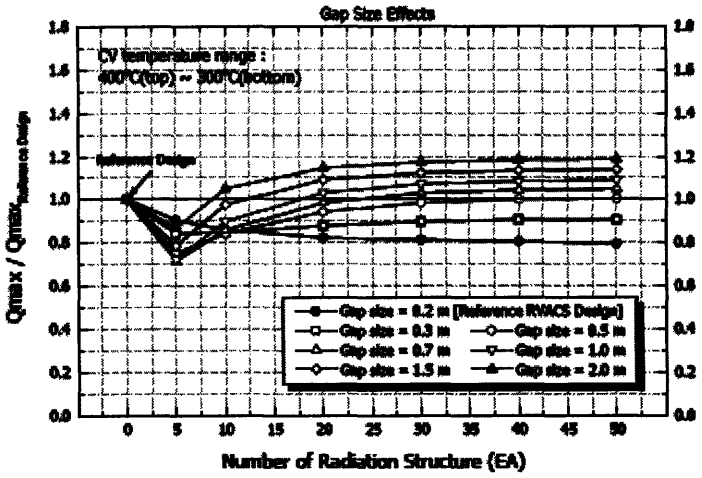

Figure 2.3. Graph of Heat removal vs. number of radiation structures for KLFR RVACS design. From Eoh et al. [2005].

3. RVACS Enhancement Options

The S-PRISM, using the RVACS design with a perforated plate and boundary layer trips in the air riser, is capable of passively removing the decay heat from a 1000MWth fast reactor. At 2400 MWth, the lead cooled flexible conversion ratio reactor must utilize a number of enhancements to achieve sufficient cooling. These include:

- Increased thermal inertia of lead coolant,
- Liquid metal bond in the gap between reactor vessel and guard vessel, and
- Air side heat transfer enhancements.

The decay heat removal capability of the RVACS system is directly proportional to the surface area of the vessel. Thus, increasing the vessel size yields larger decay power that can be removed. The large size of the vessel also allows for increased thermal inertia of the lead, which allows for a longer time and a larger decrease of decay power that needs to be removed at a peak vessel temperature. However, a larger vessel increases cost and also there are manufacturing and transportability limitations. Since the constraint on the vessel size was adopted to be the size of the S-PRISM vessel, the maximum outer diameter is set to be 9.6m, and height of 19.5m [Boardman and Hui, 1999]. The diameter constraint was applied to the guard vessel outer diameter.

3.1. Gap Fill Materials

The first enhancement made over GE's RVACS system was the addition of liquid metal into the gap between the reactor and guard vessels. The S-PRISM design used argon to fill the gap, and therefore radiation was the primary mode of heat transfer to the inner wall of the guard vessel. In the new design the effect of filling the gap with tin or lead

bismuth eutectic, or LBE, was examined. While this increases heat transfer to the guard vessel, the guard vessel thickness must be increased in order to bear the weight of the liquid contained within. The reactor vessel is essentially "floated" in by the gap fill in the guard vessel, resulting in a transfer of the reactor vessel mass almost entirely to the guard vessel. This results in an increase in guard vessel thickness if the vessel is to be able to withstand a seismic event, as analyzed in Section 6.2.

Lead-bismuth was originally considered, as it was the metal of choice for the ABR [Hejzlar et. al., 2004]. Tin was also considered, since it has a slightly higher thermal conductivity and is less dense, reducing the need for a heavy guard vessel. A drawback to this, however, is that the reactor vessel would bear a greater percentage of the weight, and would therefore need to be supported. This resulted in the ultimate decision to use LBE as the gap bond material.

For the purposes of modeling, heat transfer through the liquid metal bond was considered to be through conduction only. Some convection of the metal should occur as well, making this a conservative approximation.

3.2. Fins

Several additions to the air side of the RVACS heat exchanger were explored. The first was the addition of vertical fins welded to the exterior of the guard vessel. Appendix A explains the computer code developed and used to model this system, and Figure 3.1 shows the geometry of the fins.

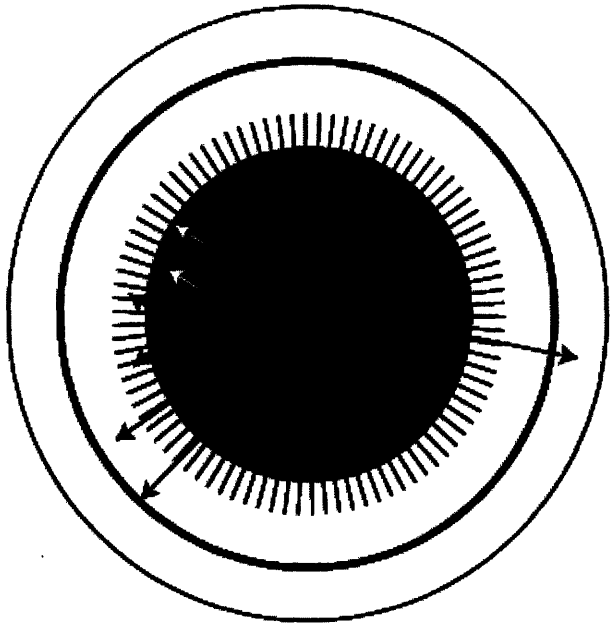

Figure 3.1. Overhead view of RVACS geometry, with added fins.

The fins add significant heat transfer area to the vessel and also could potentially add some stiffness and rigidity to the guard vessel, which could improve performance in a seismic event; however, attaching the fins would be very difficult. Assuming each fin would need to be welded on both sides, it would require about 40 meters of weld per fin. With several hundred fins needed to provide sufficient cooling, this could quickly lead to unrealistic construction requirements. Additionally, the stress imparted on the vessel by the welds would need to be considered, and could lead to quality assurance problems if conducted in the field, rather than assembled in a factory. Furthermore, annealing of welds would significantly increase the complexity of construction.

3.3. Dual-level Air Riser

Another air-side enhancement considered was the multiple-stage RVACS, where air would be introduced at two points vertically along the guard vessel, as shown in Figure 3.2. This would benefit the heat transfer by increasing the temperature difference between the hot guard vessel and the cool air along the upper surface of the guard vessel. This system would not need to be attached to the guard vessel, and could be used in addition to any other combination of heat transfer enhancements. Disadvantages to the design include an increase and complexity and cost.

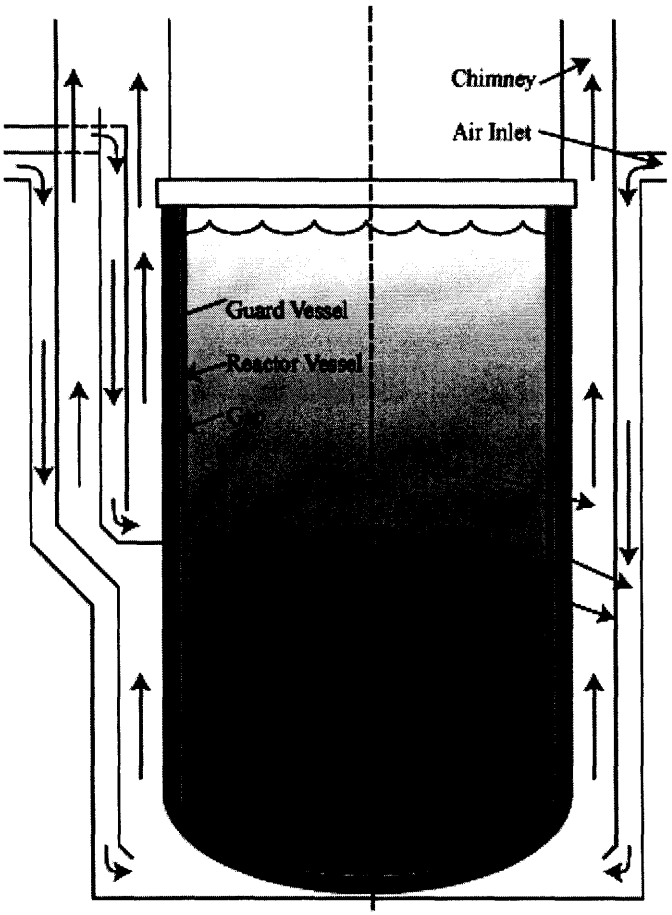

Figure 3.2. Representation of air flow in normal RVACS (right), and split-level RVACS (left.)

The split levels were modeled as two separate RVACS, each with half the number of chimneys and inlets, and half of the total heated length. The bottom level was modeled with increased chimney and inlet ducting as well, to model the geometry changes.

3.4. Perforated Plate

In GE's S-PRISM design a perforated plate was added to the air riser to provide an additional surface for the guard vessel to radiate energy to, and two additional surfaces from which the heat can be convectively removed, as shown in Figure 3.3. The perforated plate is an appealing enhancement because it does not touch the guard vessel, eliminating the possibility of compromising the integrity of the vessel during construction and assembly. The perforated plate does present a number of problems in the calculation

of the decay heat removal capacity of the RVACS system, however, and could also reduce the heat transfer if the guard vessel outer wall is not hot enough by increasing the pressure drop through the hot air riser.

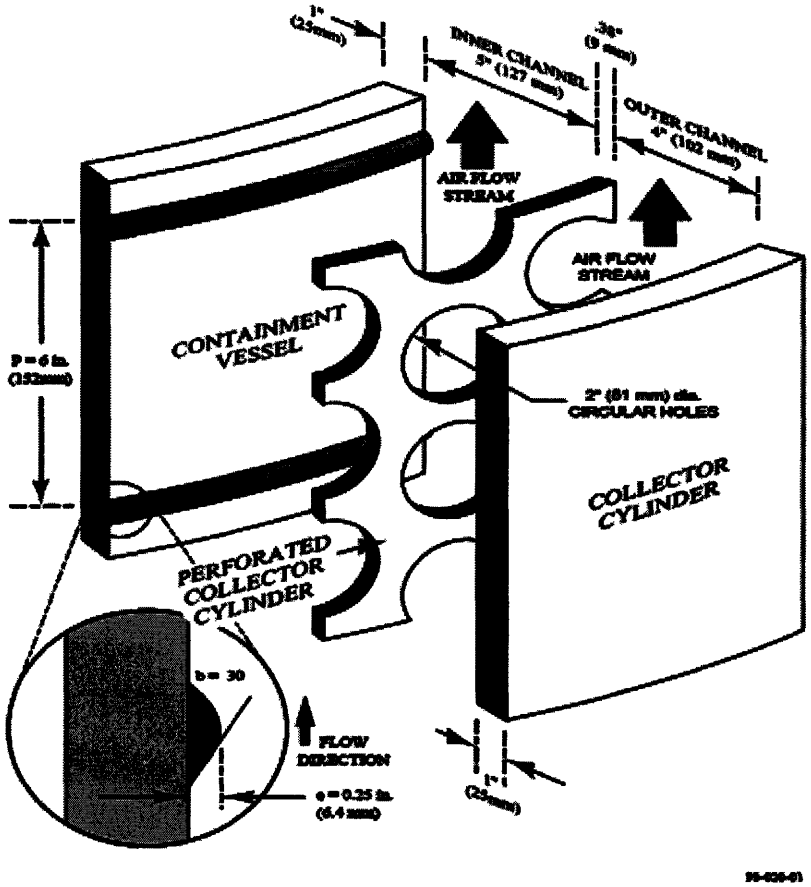

Figure 3.3. RVACS hot air riser with boundary layer trips and perforated plate. (from Boardman et al, 2000)

For the purposed of modeling the perforated plate, several simplifications were made. The surface area of the perforated plate was added to the calculation of hydraulic diameter, and radiation heat transfer between the perforated plate and both sides of the riser was calculated in addition to radiation between the guard vessel outer wall and the separator plate (referred to as the containment vessel and the collector cylinder by GE).

Turbulence caused by the perforations and boundary layer trips was ignored, and complete mixing between sides of the plate was used as an approximation.

3.5. Dimples

A fourth air-side enhancement that was examined was the addition of spherical indentations, or dimples, to the exterior of the guard vessel and potentially the separator plate as well. Dimples have been studied in recent years, with very promising results showing large heat transfer enhancement with relatively small friction factor increase. The heat transfer enhancement is due to a combination of increased surface area and boundary layer separation. Most studies that have been performed on dimples have been on much smaller systems, however, so only very rough calculations can be done, with simple multipliers added to the correlations for Nusselt numbers and friction factors. In order to add dimples to the hot air riser the guard vessel surface would need to be modified, which adds complexity to the construction of this vital part, however it should not be substantially more difficult than the boundary layer trips in GE's design, shown in Figure 3.3.

4. Methods

4.1. Design Success Criteria

There are several limits that constrain removable decay heat rates. The primary limiting factor is the temperature of the fuel cladding. The clad temperature limit of 725°C is lower than that for the reactor vessel, so the transient maximum vessel membrane temperature limit of 750°C is not included in the analysis. Since this scoping analysis is only being done on the bulk temperature of the coolant, if the analysis yields a maximum bulk coolant below the clad temperature limit of 725°C, the design will be considered successful. This is satisfactory because at decay heat power level the temperature drop across the clad is small, and there is little thermal resistance between the clad and primary coolant.

4.2. Steady-State Analysis Method

In order to quickly prototype enhancements to the RVACS system, a RVACS Mass Flow and Heat Rate Solver, or RMFHRS, was created in Java to compute steady-state heat removal rates for given geometries and primary coolant temperatures. A full description of the code can be found in Appendix A. In order to provide an estimate of the maximum primary coolant temperature inside the reactor vessel, a time-dependent analysis was done using steady state heat removal data provided by this code. This calculation allows for a fast comparison of different RVACS designs, and gives an idea of the viability of the designs. It does not, however, perform any calculations on primary coolant flow, and is therefore only an approximation that will need to be followed by a more rigorous analysis in RELAP5-3D.

After a design is chosen, RMFHRS is used to generate a set of steady state heat removal rates for varying lead temperatures. These points are then plotted, and an equation for heat removal rate vs. lead temperature is created from a linear best fit line, of the form:

$$\dot{Q}(T) = mT + \dot{Q}_0 \ , \tag{4.1}$$

where T is bulk coolant temperature measured in °C, and $\dot{Q}$ is heat removal rate, measured in watts. Q_0 is the theoretical heat removal rate at a lead temperature of 0°C, and m is the increase in heat transfer rate per degree Celsius increase in coolant temperature.

Simultaneously, decay power and integrated decay power with respect to time since shutdown are generated from an 11-exponential approximation as reported in McFaden [1984] using the DECAY program, written in FORTRAN77.

Using Excel, a discrete-time step analysis is conducted on the bulk coolant temperature. For a time step, Δt, the increase in coolant temperature is calculated from:

$$T_j = T_{j-1} + \frac{\left(\dot{Q}_{in,j-1} - \dot{Q}_{out,j-1}\right)\Delta t}{mc_p}, \tag{4.2}$$

where T_j is the temperature at time t, T_{j-1} is the temperature at time t-Δt, $Q_{in,j-1}$ is the decay heat rate at time t-Δt from the DECAY code, $Q_{out,j-1}$ is the decay heat removal rate at time t-Δt, calculated from Eq. B-1 at temperature T_{j-1}, m is the total mass of lead coolant in the vessel, and c_p is the specific heat capacity of lead at constant pressure.

Time steps were chosen that were suitably small as to limit the rounding errors, and enough were chosen to model the behavior of the system throughout the transient, until temperatures were approximately constant. The starting temperature was chosen to be the core inlet temperature for two reasons. First, this provides a conservative estimate of

the operating temperature of the decay heat removal system, as this is the lowest coolant temperature in the reactor at the moment of shutdown, and secondly, the dual-level design of the primary coolant flow path is such that the coolant that comes in contact with the vessel during normal operation has already passed through the supercritical CO_2 heat exchangers, and so is cooled to nearly the core inlet temperature.

In order to predict the core outlet temperature during the transient, it was assumed that the temperature difference in the primary coolant existing across the core during normal operation, 92°C was maintained during the transient heat up. Thus, the lowest coolant temperature was used to model the operation of the RVACS, but the highest coolant temperature is used to gauge maximum clad temperature.

Table 4.1 Description and Naming of Cases

Case No.	Stages[1]	Air-side Enhancement
1A	1	None
1B	2	
2A	1	Fins[2]
2B	2	
3A	1	Conservative Dimples[3]
3B	2	
4A	1	Optimistic Dimples[4]
4B	2	
5A	1	Perforated Plate
5B	2	

1. A value of "1" refers to a normal RVACS, whereas "2" refers to the split level design shown in Section 3.3
2. Case has 200 axial fins with thickness 2 cm and length 15 cm.
3. Assumes a bare-walled RVACS with Nu/Nu_0 of 2.0 and f/f_0 of 2.8
4. Assumes bare-walled RVACS with Nu/Nu_0 of 2.2 and f/f_0 of 1.4

4.3. Case Descriptions

In order to determine the best performing heat transfer enhancements for the RVACS, ten cases were run in the nodal analysis code discussed in Appendix A. The cases, shown in Table 4.1, were chosen to illustrate the effects of different configurations for the hot air

riser. It was apparent from inspection that GE's approach of filling the gap between the guard and reactor vessel would not alone be sufficient for the increased power rating of the FCR, and therefore all cases studied have incorporated a liquid lead-bismuth gap fill. Additionally, all cases share the properties depicted in Table 4.2. Paired cases have the same properties with the exception of the number of stages. Those with 2 stages have the multi-level design described in section 3.3, while those marked 1 have the standard RVACS riser layout.

Table 4.2 Description of Initial Design

Geometry:	
Vessel:	
Reactor Vessel Inner Diameter	9.24 m
Reactor Vessel Thickness	5 cm
Reactor/Guard Vessel Gap	3 cm
Guard Vessel Thickness	10 cm
Guard Vessel Outer Diameter	9.6m
Collector Cylinder Thickness	1 cm
Downcomer Gap	80 cm
Vessel Active Heated Length	19.5 m
Air chimney:	
Height	20 m
Diameter	6.0 m
Number	4 [1]
Air intakes:	
Length	3.0 m
Diameter	6.0 m
Number	4 [1]
Operating Parameters:	
Air Inlet Temperature	35 °C
Lead Temperature Profile	Uniform
Lead Convection Coefficient	2000 W/m^2K
1. In the split-level design, 2 intakes and 2 chimneys are used for each level	

4.3.1. Bare RVACS

Cases 1A and 1B are provided as a baseline comparison for RVACS with no air-side enhancements. These cases also illustrate the effect of the multi-level RVACS.

Radiation heat transfer from the guard vessel outer wall is considered in the heat transfer calculation, and the Nusselt numbers and the friction factors are described by equations 6 and 19, respectively, in Appendix A.

4.3.2. Fins

Cases 2A and 2B have 200 axial fins on the guard vessel which are 15 cm long and 2 cm wide, as shown by dimensions L and W in Figure 4.1. Radiation is taken into account from the guard vessel wall to the separator plate, and from the fin tips to the separator plate using bracketing methods rather than direct calculation of view factors.

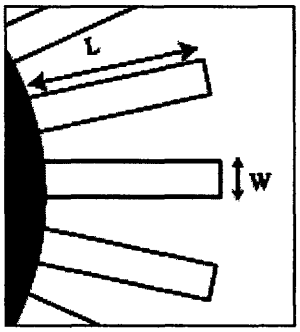

Figure 4.1. Illustration of fin geometry.

4.3.3. Perforated Plate

Cases 5A and 5B incorporate a perforated plate in the hot air riser, similar to GE's S-PRISM design. The RMFHRS model for these cases contains many simplifications in order to increase the calculation efficiency, described in Appendix A. Ultimately this leads to unexpected results, and this model will need to be refined, as discussed in Section 6.1. The current model, however, assumes a thermal emissivity, ε, of 0.8 for all surfaces. The plate is perforated so that 40% of its surface is removed to allow some of the heat to be transferred through the perforated plate to the separator plate directly by thermal radiation.

4.3.4. Dimples

Cases 3A, 3B, 4A, and 4B use estimates for the effect of dimples on the Nusselt number and pressure drop by looking at experimental data to find the most conservative and most

optimistic case. Research on dimpled heat exchangers has been mostly confined to the turbine industry, where flows are generally in much smaller passages, and therefore at lower Reynolds numbers than those being considered for the RVACS system. Unfortunately, this means that only rough estimates and a general bracketing of values can be used for calculating the enhancement effects of dimples on the wall of the guard vessel and separator plate. Of the experiments studied, Moon and Lau's had the least promising results; that is, the lowest Nusselt number augmentation with the highest friction factor increase, as seen in Figure 4.2. These tests, while calculated at lower Reynolds numbers than experienced in the RVACS hot air riser, provide a rough estimate of the lower bounds expected. Table 4.3 provides a description of the dimpled design parameters for both the most conservative estimate and the most optimistic estimates used in the model. Attempts to refine this model have been performed, and are described in Section 6.1.

Table 4.3 Description of Dimpled Design

Conservative Estimate:	
Nusselt Number Augmentation	2.0
Friction Factor Augmentation	2.8
Optimistic Estimate:	
Nusselt Number Augmentation	2.2
Friction Factor Augmentation	1.4

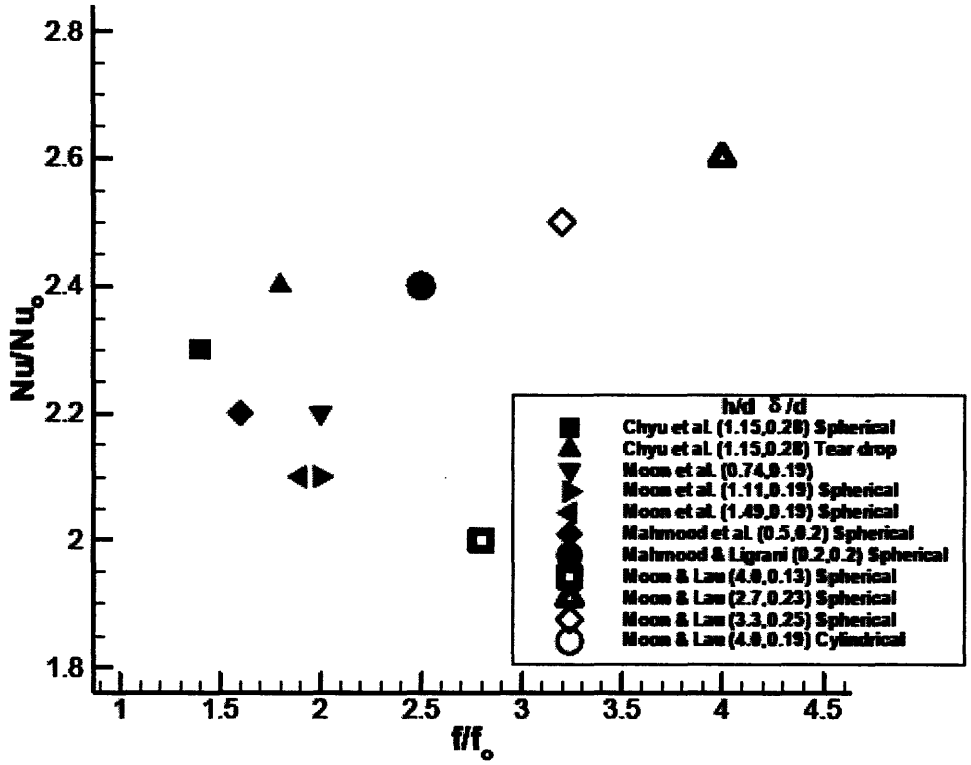

Figure 4.2. Past results of calculations on dimples by various researchers (Patrick, 2005). The lowest value (the hollow square, Moon & Lau(4.0,0.13) Spherical) was used as a conservative estimate of Nusselt number and friction factor augmentation possible at higher Reynolds numbers, and the highest performance case (the solid square, Chyu et al. (1.15,0.28) Sperical) was used as the optimistic case. In the ratios h/d and δ/d, h refers to the height of the channel, d is the diameter of the dimple, and δ is the dimple depth.

5. Results and Discussion

5.1. Air Riser Optimization

For each case a series of runs in RMFHRS were completed using a constant vessel bulk lead temperature of 600°C, with a range of riser widths. From these results the riser size that maximized heat transfer was chosen. The results are shown in Table 5.1.

Table 5.1 Optimized Riser Widths at 600 °C bulk lead temperature

Case No.	Optimized Riser Width
1A	0.29 m
1B	0.19 m
2A	0.40 m
2B	0.28 m
3A	0.41 m
3B	0.27 m
4A	0.35 m
4B	0.23 m
5A	0.39 m [1]
5B	0.26 m [1]

1. Perforated plate is placed in the center of the riser; value displayed is total riser width

5.2. Results

Following the optimization of the riser width, the air-side mass flow rate for the RVACS was calculated using the same parameters in RMFHRS. The results, shown in Table 5.2, represent the equilibrium point between pressure drop and buoyancy forces described by Equation 12 in Appendix A. The flow rates for a bulk lead temperature of 460°C are indicative of what could be expected during normal operation of the plant, while 600°C is around the temperatures reached during passive shutdown of the reactor.

The decay heat removal rate results are shown in Figure 5.1. By comparing the multi-level cases to the associated single-stage RVACS cases it is found that the average increase due to the additional riser is 7 ± 2%.

Table 5.2 Air Mass Flow Rates at 460 °C and 600 °C

	Cooling Air Mass Flow Rate	
Case No.	460 °C [1]	600 °C [1]
1A	131 kg/s	145 kg/s
1B	171 kg/s [2]	190 kg/s [2]
2A	141 kg/s	153 kg/s
2B	184 kg/s [2]	200 kg/s [2]
3A	140 kg/s	153 kg/s
3B	186 kg/s [2]	203 kg/s [2]
4A	158 kg/s	172 kg/s
4B	208 kg/s [2]	227 kg/s [2]
5A	119 kg/s	139 kg/s
5B	149 kg/s [2]	168 kg/s [2]

1. Bulk lead temperature
2. Total Mass Flow Rate (sum of both risers)

The maximum bulk coolant temperature during shutdown is shown in Figure 5.2, calculated from the DHR rate results using the method described in Section 4.2. The dark line at 725°C indicates the clad temperature limit. Since the thermal resistance between the clad and the coolant is very low, it is assumed that the clad will be negligibly hotter than the coolant. The only cases that remain below this limit are 3B, 4A, and 4B. These represent, respectively, 2-stage conservative dimples, 1-stage optimistic dimples, and 2-stage optimistic dimples.

5.3. Discussion

Ultimately, three cases were found to meet the success criteria set forth in Section 4.2. These cases represent the spectrum of dimpled wall performance that can be expected for different geometries. This result is very promising, as it indicates that given the flexibility to design and optimize the hot air riser in the RVACS these results could likely be replicated.

One notable anomaly in the results is the lack of performance by the perforated plate. The model used to describe the dynamics of the situation, described in Appendix A, seem to indicate that the pressure drop increase outweighs any heat transfer benefits of adding the plate; however, a number of important simplifications were made to the model to enable the program to run quickly. It is thought that this result may be erroneous, and it will be necessary to refine the model in future work. One possible way to do this will be to model the perforated plate in the computation fluid dynamics code Fluent, which is described in Section 6.1. This would also hopefully create some insight on how the turbulence caused by the dimples interacts with the plate's perforations.

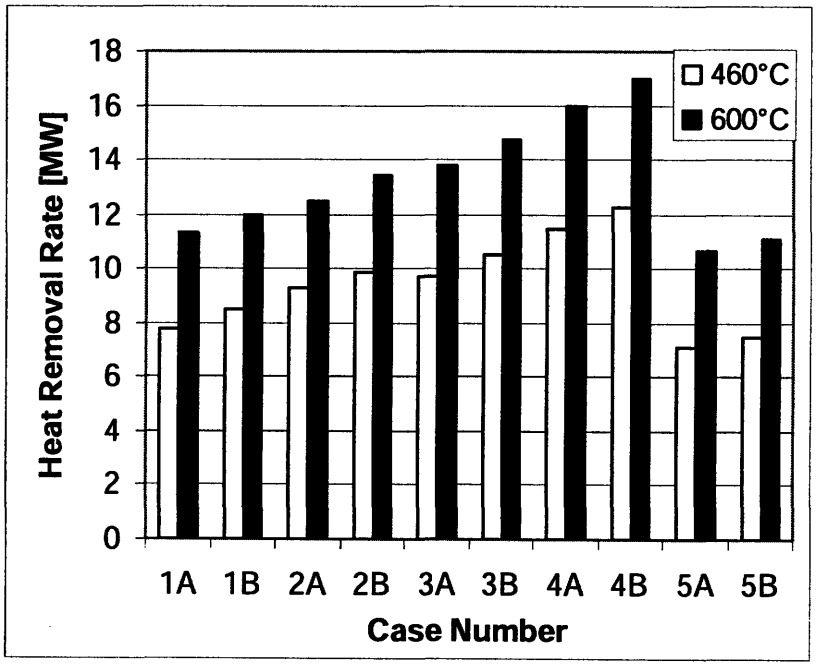

Figure 5.1 Decay Heat Removal Rates at 460°C and 600°C bulk lead temperature

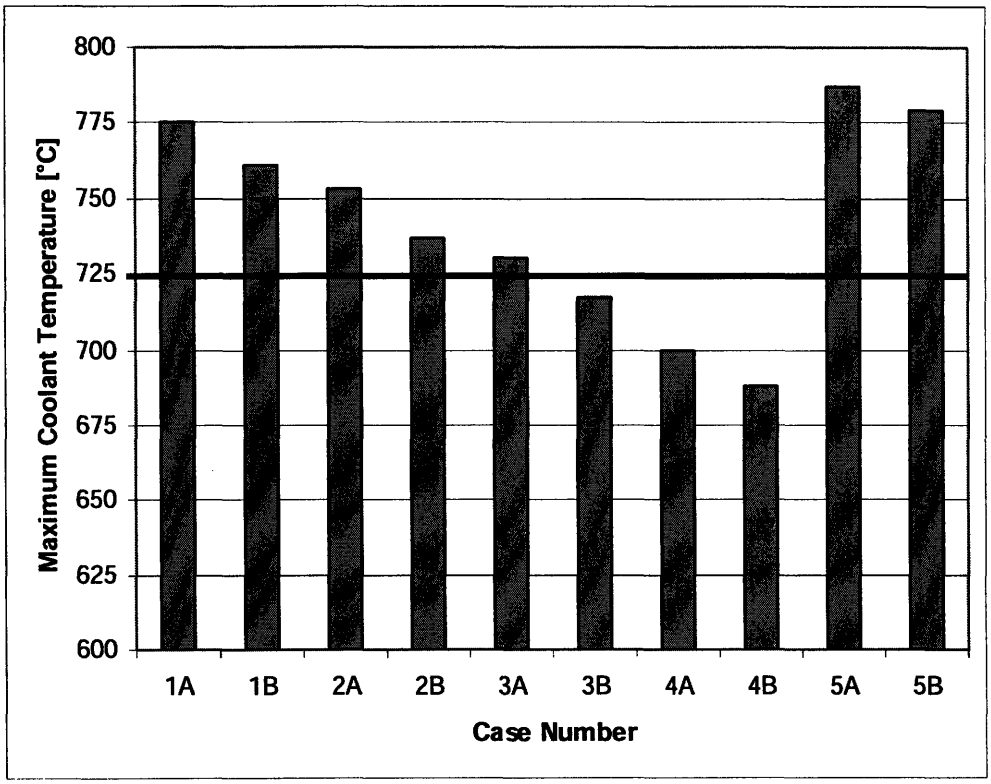

Figure 5.2 Maximum bulk primary coolant temperature achieved during passive decay heat removal shutdown event. The darkened line indicates the maximum clad temperature limit.

6. Other Work

6.1. Flow Modeling in Fluent

As the model used to represent the heat transfer and pressure drop effects of the dimples created large margins of uncertainty, work was performed to refine these results using a Computational Fluid Dynamics (CFD) code called Fluent. It was immediately realized that, with the range of options available for modeling heat transfer and viscous effects within Fluent it would be necessary to create a benchmark test using experimental data to confirm that Fluent was capturing all of the intricacies of the dimples' effect on the fluid flow. In order to accelerate the process, a pair of papers was found that demonstrate an attempt to recreate experimental data for dimple performance using Fluent. While the authors were ultimately unable to recreate the results seen in the laboratory, the papers were used as a starting point and source for laboratory-derived experimental results.

The laboratory experiment performed by Burgess, Oliveira, and Ligrani experimentally measured pressure drop and localized and global Nusselt numbers for a specific dimple geometry. The setup used included a 1.22m long, smooth-walled inlet duct of the same cross section as the dimpled section, to insure that entrance effects were not affecting the flow. This was followed by a 1.233m long, 0.411m wide, and 5.08cm tall duct with 29 rows of dimples on the bottom surface, as shown in Figure 6.1. This surface was heated to generate a heat flux of 625 W/m2, and air was blown through the channel at Reynolds numbers between 10,000 and 25,000. The dimples were machined to be 1.524 cm deep and 5.08 cm across, as shown in Figure 6.2.

The authors of the study using CFD to try to replicate the results were ultimately unable to predict the Nusselt number enhancement effect. The global Nu/Nu_0 found by Won and Ligrani were not explicitly calculated; however local Nusselt number ratios were found to

be between 0.8 and 1.3. This is a vast under-prediction of the experimental data, which indicate a Nu/Nu0 ratio of between 2.5 and 2.7. As this is the primary result of interest, it was clear that it would be necessary to try another approach within Fluent if a more representative solution was to be found.

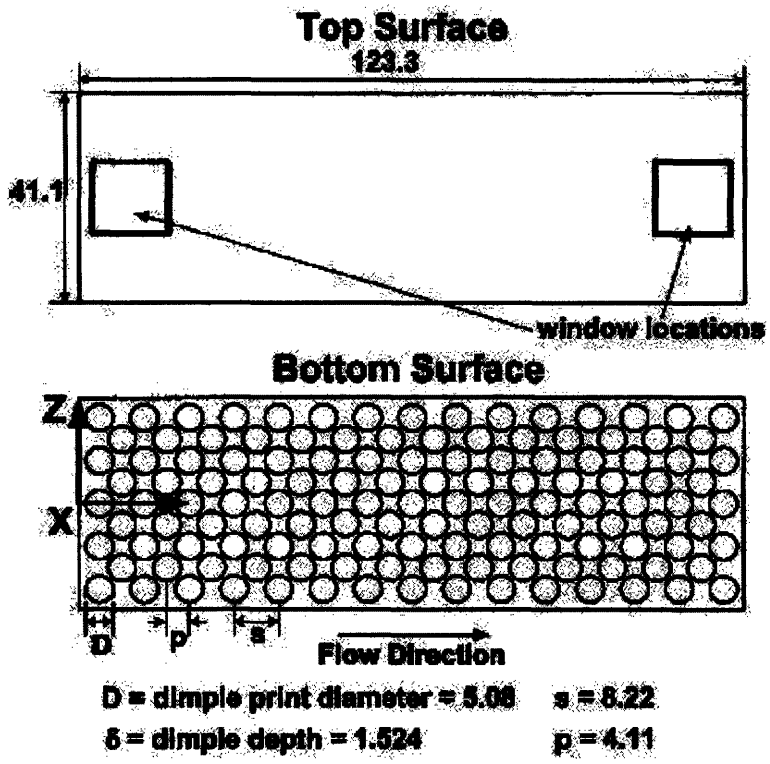

Figure 6.1. Diagram of dimple geometry. All measurements in cm. From Burgess et al. [2003].

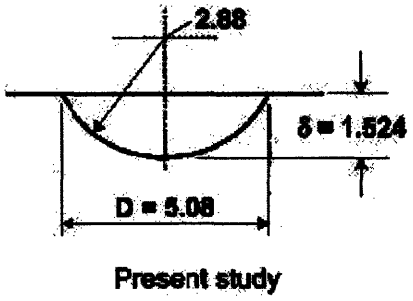

Figure 6.2. Diagram of individual dimple. All measurements in cm. From Burgess et al. [2003].

Won and Ligrani used a large mesh and flow volume to generate their solutions, modeling the entire inlet region and dimpled channel with approximately 1,000,000 mesh volumes. In order to improve the model performance a grid with much greater refinement was desired. As the computational resources necessary to run a large geometry with a small mesh were prohibitive, the decision was made to switch to a smaller geometry and use Fluent's built-in periodic flow conditions to simulate the performance of those dimples located beyond any entrance-effect regions. This boundary condition forces the inlet flow to conform to the outlet flow, simulating the fully-developed region. This allowed the use of mesh points over 100 times smaller than Won and Ligrani's model. Furthermore, this mesh was refined using the "adapt mesh" feature in Fluent, where the code automatically divides cells that have large gradients in any of a number of properties. One full dimple was modeled in addition to four one-quarter dimples, as shown if Figures 6.3 and 6.4.

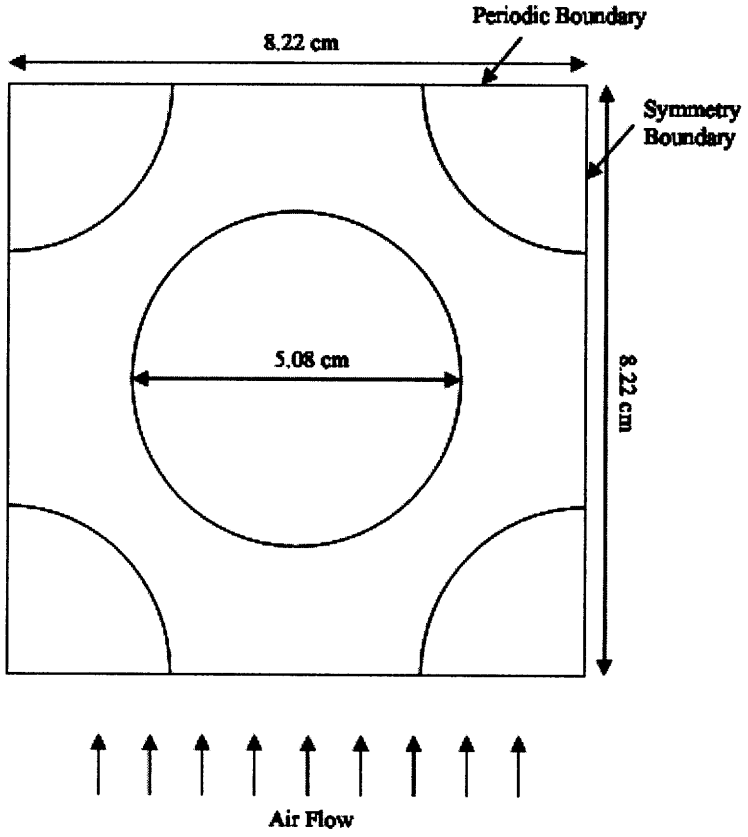

Figure 6.3. Diagram of lower plate geometry with boundary condition designations.

The results from the literature also showed that it would be unlikely that proper results could be found using the k-ε model. Thus a switch was made to modeling turbulence with the Reynolds Stress Model, or RSM. RSM solves 7 equations in addition to the Navier Stokes equations when iterating to find a solution. This method is superior for situations with large turbulence effects, as well as those with boundary layer separation. The model was used without wall functions, fully resolving the boundary layer.

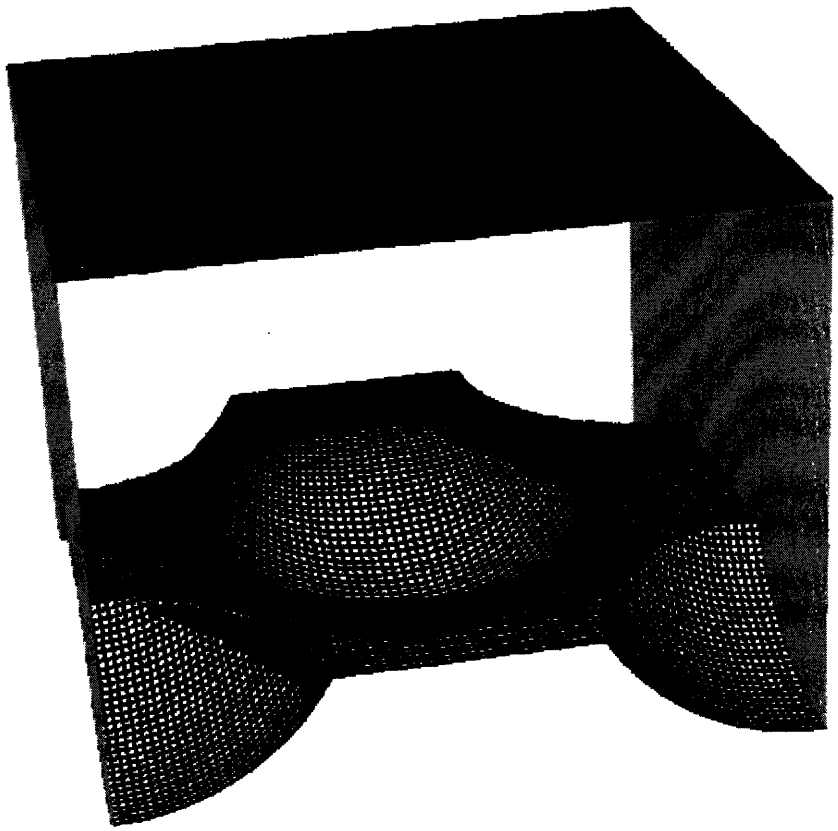

Figure 6.4. Meshed dimple geometry in Fluent. Flow is into the page. Side walls have symmetry boundary conditions imposed.

The dimpled geometry was iterated in Fluent until the solution converged. The mesh was then refined twice on both pressure and temperature gradients. This result produced a globally average Nusselt number ratio, Nu/Nu_0, of 1.5 when the Dittus Boelter correlation was used as Nu_0; considerably less than the expected value of 2.5 from the laboratory experiment, as shown in Table 6.1. Furthermore, a comparison of friction

factor ratios, f/f_0, showed even worse agreement, as the CFD code predicted f/f_0 of 5.4, whereas the laboratory result showed a value of 1.8.

Table 6.1. Comparison of Fluent periodically calculated dimple results to laboratory results

	FLUENT	Laboratory
Nu/Nu_0[1]	1.5	2.5
f/f_0	5.4	1.8
[1]Nu_0 calculated from Dittus-Boelter		

It was decided that an important test of Fluent's performance and to confirm that the correct boundary conditions and flow models were chosen would be a comparison of a smooth-walled channel to commonly used correlations. This was never performed by Won and Ligrani for their case. A rectangular prism was thus modeled in Fluent with dimensions 8.22cm x 8.22cm x 5.08cm as the flow volume, the same as the periodic dimple mesh. This was run with the same boundary conditions and mass flow rate as the periodic dimple model. The mesh was refined on both pressure and temperature gradients, but the results still showed a large error in both pressure drop and Nusselt number as compared to standard correlations for turbulent flow. It was not until the grid was greatly refined along the velocity gradients was a satisfactory solution converged upon for the friction factors, although the Dittus Boelter correlation still showed a 18% error when compared with the Fluent solution. Hence it was decided to compare to another, generally more accurate, correlation proposed by Gnielinski [1976]. This gave excellent agreement, with an error of only 5%. While this confirms the successful modeling in Fluent of the flat plate, it does not resolve the issues with Nusselt number agreement between the dimpled case and the laboratory results, since Burgess et al. compared the experimentally determined Nusselt number to the Dittus Boelter correlation.

Table 6.2. Comparison of flat-plate model in FLUENT to various correlations

f_{fluent}/f_0	1.1
$Nu_{fluent}/Nu_{0\text{-DittusBoelter}}$	0.82
$Nu_{fluent}/Nu_{0\text{-Gnielinski}}$	0.95

Judging from the experience using the RSM and periodic boundary conditions to model a flat plate it is possible that the RSM model could be used to solve the dimpled geometry using a much refined mesh. Unfortunately there was not sufficient time to continue to pursue this, and therefore it will be left for future work. In the event that the RSM model does not show sufficient agreement, the next option will be to move to a Large Eddy Simulation, or LES, model in Fluent. LES requires much greater computational resources than either the k-ε or RSM models and will thus likely require a long period of time before conclusions can be drawn.

The final step after confirming laboratory tests using the CFD code will be to model different dimple geometries using the channel height and Reynolds numbers seen in the hot air riser of the RVACS. Using Fluent a number of different geometries could be prototyped to see the effect on heat transfer and pressure drop. From these results a correlation could be created and used in either the RMFHRS or Fluent to determine the total heat transfer possible for the hot air riser. Furthermore, Fluent could be used to model both the radiation effects of the perforated plate, as well as the turbulizing effect of the perforations on pressure drop and Nusselt number, greatly reducing any uncertainties that remain in the current RVACS design.

6.2. Seismic Accident Analysis

The first enhancement made over GE's RVACS system was the addition of liquid metal into the gap between the reactor and guard vessels. The S-PRISM design used argon to fill the gap, and therefore radiation was the primary mode of heat transfer to the inner wall of the guard vessel. In the new design the effect of filling the gap with tin or lead bismuth eutectic was examined. This causes the reactor vessel to "float" within the guard vessel, resulting in a transfer of most if not all of the reactor vessel weight directly to the guard vessel. While this increases heat transfer to the guard vessel, the guard vessel thickness must be increased in order to bear the weight of the liquid contained within. Lead-bismuth was originally considered, as it was the metal of choice for the ABR [Hejzlar et. al., 2004]. Tin was also considered, since it has a slightly higher thermal conductivity, and is less dense, reducing the need for a heavy guard vessel. A drawback

to using a lighter metal, however, is that the reactor vessel would bear a greater percentage of the weight, and would therefore need to be supported and possibly thickened. Pure lead was not included in the analysis, as at the temperatures experienced during normal operation it would be in the solid phase, and then would melt as the vessel temperature increased in a passive DHR shutdown. This would introduce a plethora of new complications to the design and is thus undesirable.

Seismic analysis was carried out using a non-dimensionalization method described by Buongiorno and Hawkes [2003] and described in Appendix B. Their method returned the results in Table 6.3 for a non-seismically isolated reactor vessel in a 0.5g peak ground acceleration earthquake. The maximum allowable stress for SS316 from ASME code (Level D Service Loadings) is 263.1 MPa. This limit is not achieved until the guard vessel thickness is increased to 22 cm and 15.1cm for lead-bismuth and tin filled gaps, respectively.

Table 6.3 Response of lead-filled guard vessel in 0.5g magnitude earthquake

Gap Fill	Vessel Thickness [cm]	1st Mode Frequency [Hz]	Peak Acceleration [m/s^2]	Peak Stress Intensity [MPa]
Lead/ Bismuth	10	3.3	18.8	603
	15	4.1	18.4	393
	20	4.7	18.1	288
	22	5.0	18.0	260
Tin	10	4.0	18.5	407
	15	4.9	18.1	264
	20	5.7	17.7	193

Thermal constraints, however, necessitate a vessel around only 10 cm thick; therefore, it is necessary to consider seismic isolation schemes.

Buongiorno and Hawkes found that the 1st mode of oscillation during an earthquake was a simple lateral bending, and that this mode is the major contributor to the total peak stress intensity. Therefore, it might be possible to significantly reduce the stress by protecting the vessel from lateral motions near the base. Additionally, GE's S-PRISM

design utilizes seismic isolators, which GE claims reduce the lateral load by a factor greater than 3. Taking this into account, it would then be possible to use a 10 cm thick guard vessel with a LBE filled gap without compromising the guard vessel integrity in the event of an earthquake.

6.3. Static Stress Analysis

While Figure 5.2 shows that clad temperature constraints can be met during a passive shutdown of the core, it is also important to ensure that temperature constraints on the reactor and guard vessels are met. Thus, both configurations of the optimistic and conservative dimples cases were examined at their estimated temperature peak from Figure 5.2 to determine the theoretical maximum vessel temperatures. The results are shown in Table 6.4. The reactor vessel maximum temperature is highly dependent on the heat transfer coefficient between the lead coolant and the wall, which is only roughly estimated in the RMFHRS analysis. As the reactor vessel is not a weight bearing structure, it is in considerably less danger of rupture due to elevated temperatures.

Table 6.4 Maximum Vessel Temperatures During Passive Decay Heat Removal

RVACS Type	Maximum Coolant Temperature During Passive Shutdown	Reactor Vessel Max Temperature	Guard Vessel Max Temperature
Conservative Dimples 1-Stage	730 °C	715 °C	610 °C
Conservative Dimples 2-Stage	717 °C	702 °C	593 °C
Optimistic Dimples 1-Stage	700 °C	684 °C	568 °C
Optimistic Dimples 2-Stage	688 °C	672 °C	554 °C

The four cases shown in Table 6.4 were analyzed for compliance with ASME Level C service limits. In order to perform this analysis the primary membrane stress intensity was calculated to be 105.3 MPa using the formulae from Buongiorno [2001]. Finally, the time needed for the passive RVACS system to reduce the primary coolant temperature to normal operation levels was found to be approximately 70 hours, as seen in Figure 6.5. Using the values for temperature (610°C) and duration of shutdown (70 hours), it can be seen that even for the 1-stage conservative dimples case the vessel will satisfy the service limits set forth by ASME for a SS316 vessel (113 MPa), seen in Figure 6.6, proving that the vessel primary membrane stress intensity (105.3 MPa) is not the limiting factor during a passive decay heat removal scenario.

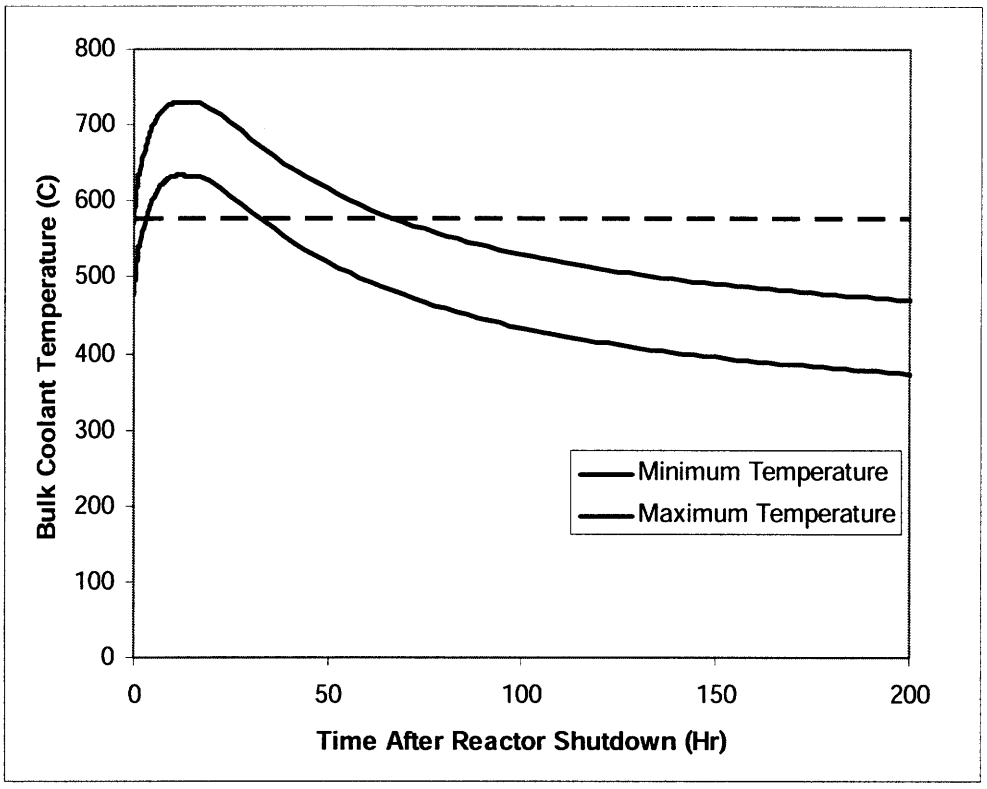

Figure 6.5. Bulk coolant temperature during passive shutdown for 1-Stage conservative dimples RVACS. Dotted line shows high temperature during normal operation.

TABLE I-14.4B
S_t — ALLOWABLE STRESS INTENSITY VALUES, MPa, TYPE 316 SS (CONT'D)

SI Units											
Temp., °C	1 hr	10 hr	30 hr	10^2 hr	3×10^2 hr	10^3 hr	3×10^3 hr	10^4 hr	3×10^4 hr	10^5 hr	3×10^5 hr
427	143	143	143	143	143	143	143	143	143	143	143
454	142	142	142	142	142	142	142	142	142	142	140
482	141	141	141	141	141	141	141	141	139	137	133
510	139	139	139	139	139	138	138	136	132	127	121
538	137	137	137	137	137	134	131	125	121	112	97
566	134	134	132	129	126	121	116	110	103	86	74
593	132	131	128	123	119	114	110	96	79	66	54
621	128	122	119	113	106	98	90	75	61	50	41
649	123	116	109	98	85	73	65	57	48	38	31
677	118	105	93	79	68	57	50	43	37	29	23
704	111	88	75	63	52	44	39	32	27	21	17
732	98	71	59	48	41	34	29	23	19	14	12
760	83	57	46	37	31	26	21	17	14	10	8
788	67	44	35	28	23	20	15	12	10	7	6
816	54	34	27	22	18	14	11	8	6	4	3

Figure 6.6. Table from ASME code showing stress intensity limits for 316 SS. [From Boiler and Pressure Vessel Code, 2002] By rounding to the next highest value for temperature at 621°C, and time at 10^2 hr, it can be seen that the maximum stress intensity is 113 MPa; this is below the value calculated for the FCR vessel.

7. Conclusions and Future Work

While more work is necessary to reduce the uncertainty within the different models, it appears that a modified and optimized RVACS system will be able to remove sufficient heat in the event that passive cooling of the core is necessary. Dimple performance and perforated plate modeling will be an important part of the continuing design process for this system; however, it is now possible to conclude that some combination of the elements studied will be sufficient. The most promising result is that of the conservative dimples case, whereby the least optimistic approximation of the Nusselt number and friction factor augmentation still maintains temperatures below the maximum clad limit when a double level riser is used. The final design choice will include dimples, possibly in a multiple-stage and/or perforated plate design. The design of the dimples will be left to future work, as modeling in CFD code has been unsuccessful thus far. Also left to future work is the decision on whether or not to include a perforated plate in the design of the DHR system. If further research shows it to be beneficial, it will be included to increase the margin to clad failure. The double-level riser design will also be included, as it has shown to improve the performance of the RVACS by a small yet substantial percentage.

Additional future work will include modeling the entire system using a transient analysis code, such as RELAP5-3D. This will allow for confirmation that the pseudo-steady state analysis method acts as a conservative estimate of natural circulation within the primary loop.

Work will also need to be performed to define the seismic isolation approach that will be necessary to reduce the stress on the vessel during an earthquake. If this proves to be impossible, it may be necessary to consider more radical DHR enhancements, or an

increase of vessel diameter in order to sufficiently cool the reactor during a passive shutdown.

Bibliography

Boardman C., Dubberley A., Carrol D., Hui M., Fanning A., and Kwant W., "A Description of the S-PRISM Plant," Proceedings of ICONE 8, Baltimore, MD, USA, 2000.

Boardman C.E., Dubberley A.E., and Hui M., "Optimizing the Size of the Super-PRISM Reactor", Proceedings of ICONE 8, Baltimore, MD, USA, 2000.

Boardman C.E. and M. Hui, "A Competitive Integral Fast Reactor With Enhanced Diversion Resistance (S-PRISM)", Proceedings of Global 99, Jackson Hole, WY, USA, 1999.

"Boiler & Pressure Vessel Code. An International Code. Section III, Division 1, Subsection NH (Class 1 Components in Elevated Temperature Service)." ASME, 2001

Buongiorno J. and Hawkes B.D., "Seismic Analysis of Heavy-Liquid-Metal-Cooled reactor vessels," Nuclear Engineering and Design, 228, pp. 305-317, 2004.

Buongiorno J, "Temperature Limits for Heavy-Liquid-Metal Reactor Vessels." Proceedings of the 2001 ANS Winter Meeting, Reno, 2001

Burgess N.K., Oliveira M.M., and Ligrani P.M., "Nusselt Number Behavior on deep Dimpled Surfaces within a Channel", J. Heat Transfer, Vol., 125, pp. 11-18, 2003.

Cummins W.E., Corletti M.M., Schulz T.L., "Westinghouse AP1000 Advanced Passive Plant," Proceedings of ICAPP '03, Cordoba Spain, 2003.

Eoh J.H., Kim J.B., Kim S.J., and Kim S.O., "Design and Performance of the Passive Decay Heat Removal System in a Lead-cooled Fast Reactor," Proceedings of ICAPP '05, Seoul, Korea, 2005.

Gnielinski V., "New Equations for Heat and Mass Transfer in Turbulent Pipe and Channel flow", *International Chemical Engineering*, **Vol. 16**, *No. 2*, pp. 359-387 (April 1976)

Hejzlar P., Buongiorno J., MacDonald P., and Todreas N., "Design Strategy and Constraints for Medium-Power Lead-Alloy-Cooled Actinide Burners," Nuclear Technology, 147, pp.321-343, 2004.

Patrick W. "Computations of Flow Structures and Heat Transfer in a Dimpled Channel at Low to Moderate Reynolds Number," Master's Thesis, Virginia Tech, 2005.

Todreas N.E., MacDonald P.E., Hejzlar P., Buongiorno J., and Loewen E.P., "Medium-Power Lead-Alloy Reactors: Missions for this Reactor Technology", Nuclear Technology, Vol. 147, September 2004, pp305-320.

Won S.Y. and Ligrani P.M., "Numerical Predictions of Flow Structure and Local Nusselt Number Ratios along and above Dimpled Surfaces with Different Dimple Depths in a Channel", Numerical Heat Transfer, Part A, Vol. 46, pp. 549-570, 2004.

Nomenclature

Re	Reynolds number
Nu	Nusselt number
Dh	hydraulic diameter, in m
f	Darcy friction factor
f_0	reference Darcy friction factor
Nu_0	reference Nusselt number
δ	dimple depth, in cm
H	channel height, in cm
D	dimple diameter, in cm

Appendix

Appendix A: RVACS Mass Flow and Heat Rate Solver Code Description

Problem Formulation:

In order to quickly prototype geometry changes and other enhancements to the RVACS system, a model was created in Java to return heat removal rates for given geometries and primary coolant temperatures. The design for this model is shown in Fig. A.1. Two vessels, an interior reactor vessel, and an exterior guard vessel, are separated by a gap filled with a liquid metal bond. The heat it removed by air flow down the downcomer, up through the riser, and out the chimney, which is driven by buoyancy forces caused by density changes within the air. Heat is convected by the air away from two surfaces: the guard vessel outer wall and the separator plate. Heat is transferred to the separator plate through thermal radiation from the guard wall. Heat is conducted through the reactor and guard vessels, and is modeled as a conduction process through the liquid metal gap as well, to simplify the calculations.

Assumptions:

The assumptions used by this model are:

- steady state;
- temperature of walls and vessels are considered constant in the azimuthal direction;
- the surfaces involved in radiation are grey;
- the air does not participate with respect to radiation;
- the separator plate is perfectly insulating;
- convection heat transfer coefficient is constant throughout the riser azimuthally;
- all inlet and outlet ducting is perfectly insulating;
- the convective heat transfer between the lead and the inner wall is constant throughout;
- the inner lead temperature varies linearly in the axial direction;

- heat transfer through the liquid metal gap can be modeled as conduction;
- axial radiation is neglected;
- axial conduction is neglected.

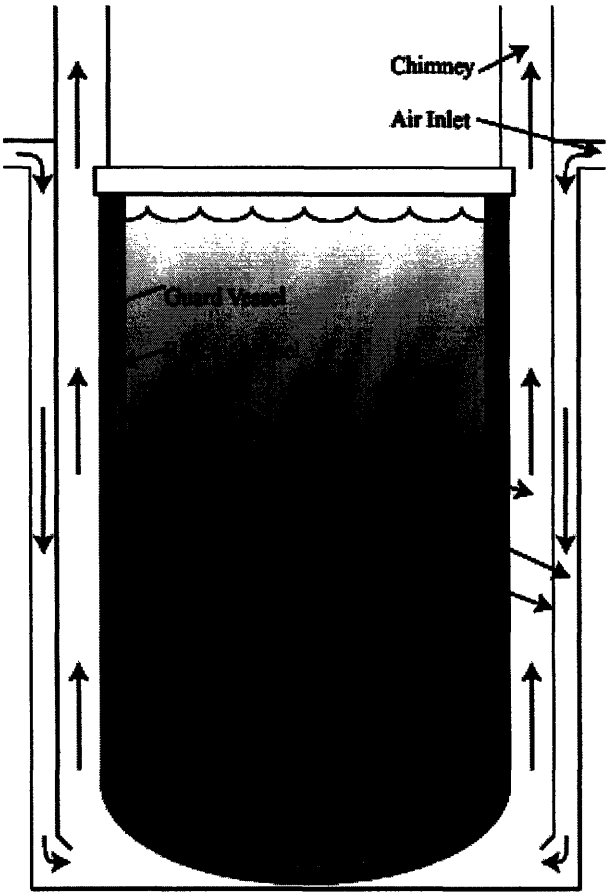

Figure A.1 Side view of RVACS system, showing air-side flow path

Energy Balances:

The code calculates the surface temperatures of both the outside of the guard vessel and the separator plate wall by iteration. For both cases, the program solves for the temperature at which the heat transferred to the surface is equal to the heat transferred away from the surface.

For the heat balance within the separator plate, the heat transfer area is divided into N_1 nodes of equal height Δx, as shown in Fig. A.2. Define the nodal surface area of the separator plate and the outer wall of the guard vessel,

$$A_{separator} = 2\pi R_5 \Delta x, \tag{A.1}$$

$$A_{guard} = 2\pi R_4 \Delta x, \tag{A.2}$$

where R_4 and R_5 are the radii of the outer wall of the guard vessel and of the separator plate, also shown in Fig. A.2,

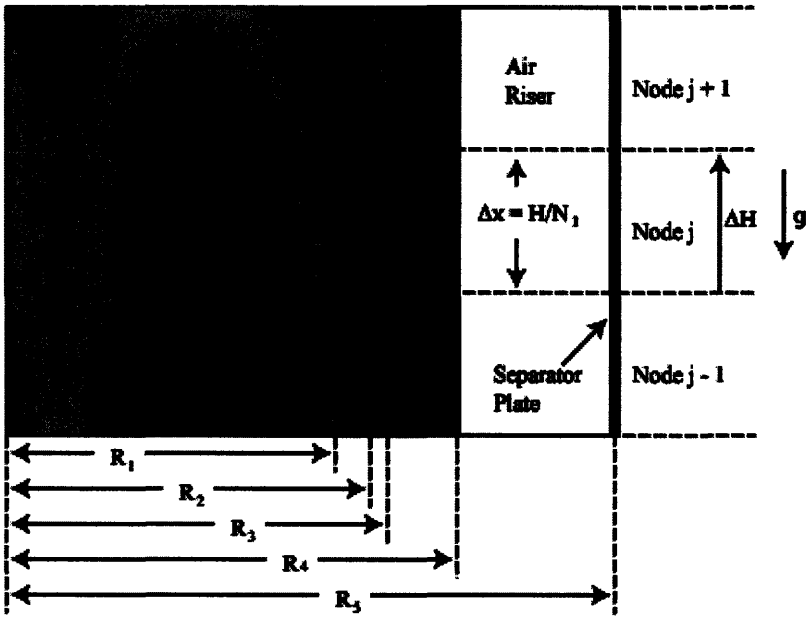

Figure A.2. Close up of RVACS geometry, and depiction of naming conventions.

The only method of heat transfer to the separator plate is through radiation from the guard vessel. The net transfer of heat to the separator plate in the j^{th} node can be calculated from:

$$\dot{Q}_{in,separator,j} = C_{guard} A_{guard} (T^4_{guard,j} - T^4_{separator,j}), \tag{A.3}$$

where $T_{guard,j}$ and $T_{separator,j}$ are the temperatures at node j of the guard wall and separator, and C_{guard} is defined as:

$$C_{guard} = \sigma \left[\frac{1}{\varepsilon_{guard}} + \frac{A_{guard}}{A_{separator}} \left(\frac{1}{\varepsilon_{separator}} - 1 \right) \right]^{-1}, \tag{A.4}$$

where σ is Boltzmann's constant, and ε_{guard}, and $\varepsilon_{separator}$ are the emissivities of the guard vessel, and separator plate.

The heat transfer from the separator plate to the air is modeled as pure convection, with a heat transfer coefficient derived from the correlation described in Eq. A.6. The heat transfer rate from the separator plate is thus:

$$\dot{Q}_{out,separator,j} = h_j \, A_{separator} (T_{separator,j} - T_{bulkair,j}) \, , \tag{A.5}$$

where $T_{bulkair,j}$ is the bulk air temperature entering the node, and h_j is the convective heat transfer coefficient calculated from a correlation developed experimentally by ANL for heat transfer in an RVACS as [Heineman et. al., 1988], [Hejzlar, 1994]:

$$h_j = 0.0229 \, \mathrm{Re}_j^{0.8} \, \mathrm{Pr}_j^{0.4} \, \frac{k_{air,j}}{D_h} \left(\frac{T_{guard,j}}{T_{air,j}} \right)^{-0.4} \left[1 + \left(\frac{z_j}{D_h} \right)^{-0.36} \right] , \tag{A.6}$$

where Re is the Reynolds number, Pr is the Prandtl number, k_{air} is the thermal conductivity of the air, D_h is the hydraulic diameter of the ducting, and z_j is the distance above the riser inlet.

Finally, to find the steady state solution equations A.3 and A.5 are set equal, and the separator temperature is solved for.

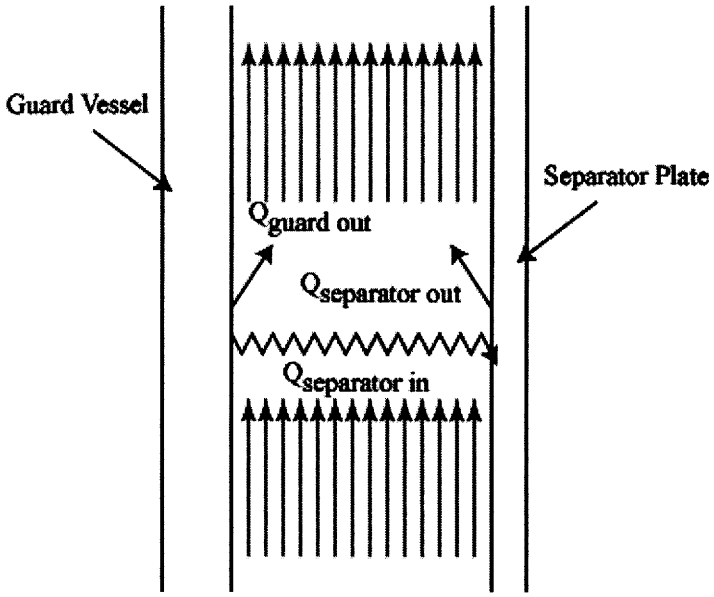

Figure A.3. Depiction of energy transfer in bare walled RVACS

The guard vessel outer wall temperature is found using the same heat-balance methodology. Heat is transferred away from the vessel by two parallel pathways: convection to the air and radiation to the separator plate, as shown in Fig. A.3. The radiation heat transfer rate is calculated in equation A.3, and the total heat transfer away from the guard vessel is:

$$\dot{Q}_{out,guard,j} = h_j \, A_{guard} (T_{guard,j} - T_{bulkair,j}) + \dot{Q}_{in,separator,j} \tag{A.7}$$

Heat transfer to the guard vessel outer surface from the hot lead primary coolant is modeled as a series of resistances between the lead temperature and the guard vessel outer wall. The resistance between the hot lead and the reactor vessel is:

$$R_{lead} = (h_{lead} \, 2\pi \, R_1 \, \Delta x)^{-1}, \tag{A.8}$$

where h_{lead} is a user defined input. The remaining three resistances can be represented as:

$$R_{cylinder} = \frac{\ln(R_{out}/R_{in})}{2\pi k \Delta x}, \tag{A.9}$$

where R_{out} and R_{in} are the outer and inner radius of the cylindrical barrier, and k is the thermal conductivity of the vessel or gap material. The total resistance is thus:

$$R_{total} = R_{lead} + R_{reactor\ vessel} + R_{gap} + R_{guard\ vessel}\ , \tag{A.10}$$

with the last three resistances on the right hand side calculated from Eq. A.9, and the total heat transfer into the guard vessel is:

$$\dot{Q}_{in,guard,j} = R_{total}^{-1}(T_{lead,j} - T_{guard,j})\,. \tag{A.11}$$

Using the same technique as is used to find the separator plate temperature, Eq. A.11 is set equal to Eq. A.7 and the guard vessel outer wall temperature is solved for.

Mass Flow Rate Determination:

The air mass flow rate is determined from a balance between buoyancy forces and pressure losses using

$$\dot{m} = \sqrt{\frac{\Delta p_b}{c}}\ , \tag{A.12}$$

where c represents the pressure drop due to form and friction losses as defined as:

$$c = \sum_{j=1}^{N}\left(K_j + f_j\frac{L_j}{D_{h,j}}\right)\left(2\rho_j A_j^2\right)^{-1}\ , \tag{A.13}$$

where N is the total number of nodes (heated and unheated), K is the form loss coefficient, f is the friction loss coefficient defined below in Eq. A.19, L is the length of the node, D_h is the hydraulic diameter, ρ is the average density of air within the node, and A is the total cross sectional area of the ducting.

The thermal buoyancy coefficient, Δp_b is defined as:

$$\Delta p_b = \sum_{j=1}^{N} \rho_j \left(\Delta \vec{H}_j \bullet \vec{g} \right), \tag{A.14}$$

where g is the gravitational acceleration, ρ is the average air density, and ΔH is the elevation change. Sign conventions followed are shown in Fig. A.2, above.

Air properties calculation:

In order to most accurately model the RVACS system, air density, specific heat, viscosity, and thermal conductivity must be modeled as functions of air temperature and/or pressure.

For density calculations, air is treated as an ideal gas. Thus a simple rearrangement of the ideal gas law yields:

$$\rho = \frac{m}{V} = \frac{P}{RT}, \tag{A.15}$$

where P is the pressure is Pascals, T is temperature in Kelvin, and R is the gas constant for air, 287 j/kg-K.

The remaining properties were calculated from formulae in Irvin [1984]. They are as follows:

$$C_p = 1034.09 - (0.284887)T + (7.816818\times10^{-4})T^2 - (4.970789\times10^{-7})T^3 + (1.077024\times10^{-10})T^4 , \quad (A.16)$$

$$k = -2.2276501\times10^{-3} + (1.2598485\times10^{-4})T - (1.4815235\times10^{-7})T^2 + (1.4815235\times10^{-10})T^3 - (1.066657\times10^{-13})T^4 + (2.47663035\times10^{-17})T^5 , \quad (A.17)$$

$$\mu = (-0.98601 + (9.080125\times10^{-2})T - (1.17635575\times10^{-4})T^2 + (1.2349703\times10^{-7})T^3 - (5.7971299\times10^{-11})T^4)\times10^{-6} , \quad (A.18)$$

where T is in units of Kelvin, C_p is the specific heat in units J/kg-K, k is thermal conductivity in W/m-K, and μ is kinematic viscosity in kg/m-s.

Pressure drop and change in temperature calculations:

To facilitate the calculation of a solution the heat exchanger is divided into a user-defined number of nodes of equal height, while the inlet and outlet ducting is divided into user specified nodes of independent lengths. The inlet air temperature and pressure for each node is provided by the node prior. All air properties are calculated at the inlet of the node, and assumed constant throughout.

Pressure drop is calculated identically for all nodes, heated and unheated. The friction factor is found from Idelchik [1986]:

$$f_j = 0.11\left(\frac{\zeta}{D_h} + \frac{68}{\mathrm{Re}}\right)^{0.25} , \quad (A.19)$$

where f_j is the fanning friction factor, where D_h is the hydraulic diameter in the j^{th} section of ducting, ζ is the sand-grain roughness of the j^{th} node, and Re is the Reynolds number, calculated at the inlet of the node. This leads to the pressure drop through:

$$P_{in,j+1} = P_{in,j} - \rho\left(f_j \frac{L}{D_h}\frac{v^2}{2} + K\frac{v^2}{2} \right) , \qquad \text{(A.20)}$$

where $P_{in,j}$ and $P_{in,j+1}$ are the pressures at the inlet and outlet of node j, ρ is the inlet density of the air, L is the length of the ducting in the node, v is the velocity at the inlet of the node, and K is the form loss coefficient.

Temperature change is calculated only for the heated section of the RVACS system. The heat transfer to the air in the node was calculated using the sum of Eq. A.7, once the guard vessel outer wall and separator plate temperatures were determined. The temperature increase of the air is then calculated from:

$$T_{out,j} = T_{in,j} + \frac{Q_{total,j}}{\dot{m}C_p} , \qquad \text{(A.21)}$$

where $T_{in,j}$ and $T_{out,j}$ are the inlet and outlet temperatures of node j, $Q_{total,j}$ is the total heat transfer to the air within the node, m is the mass flow rate, and C_p is the specific heat at constant pressure of the air, calculated at the inlet of the node.

Solution approach:

Once initiated the code generates a number of "node" objects in a queue, one for each heated and unheated node. Following this, an initial guess of the mass flow rate is made, and the buoyancy forces and pressure loss are calculated for this flow rate, as depicted in Fig. A.4. Dependent on the flow rate being incorrect, this process is iterated until the flow rate balances the buoyancy and pressure loss forces.

In order to calculate the buoyancy forces, the heat transfer rate is important to calculate the temperature increase in the air, and the resulting change in density. At each heated node, the air properties are calculated from the outlet temperature and pressure of the previous node. The guard vessel outer wall temperature is then bracketed between the

guard vessel temperature at the node prior, and the air temperature. A bisection method using energy balances then solves for the guard vessel temperature at the node, in doing so calling a bisection method on the separator plate temperature, which is bracketed between the guard vessel temperature, and the air temperature. Following completion of the bisection methods the total heat transfer to the air and the output air temperature for the node are calculated. To incorporate pressure losses due to friction forces, Eqs. A.19 and A.20 are used to calculate the outlet air pressure.

Following pressure and heat transfer calculations, the next node is called, and the process repeats. After tallying up total buoyancy and pressure forces, an adjustment to the mass flow rate is made, and the process iterates. After a suitable solution is found, the program prints the result to file.

Modification for Finned Wall Heat Transfer Calculation:

If axial fins are added to increase heat transfer, new energy pathways must be added to the energy balance equations. The fins act to conduct heat outwards from the vessel, where it can be removed through an increased surface area. This benefit must be weighed with the decreased radiative heat transfer from the guard vessel to the separator plate.

Assumptions:

The assumptions used by this model include those listed above for a bare-walled RVACS. Additional assumptions made for the fin design are:

- radiation between adjacent fins can be neglected;
- boundary layer buildup between fins is insignificant;
- there is no thermal resistance between the base of the fins and the guard vessel.

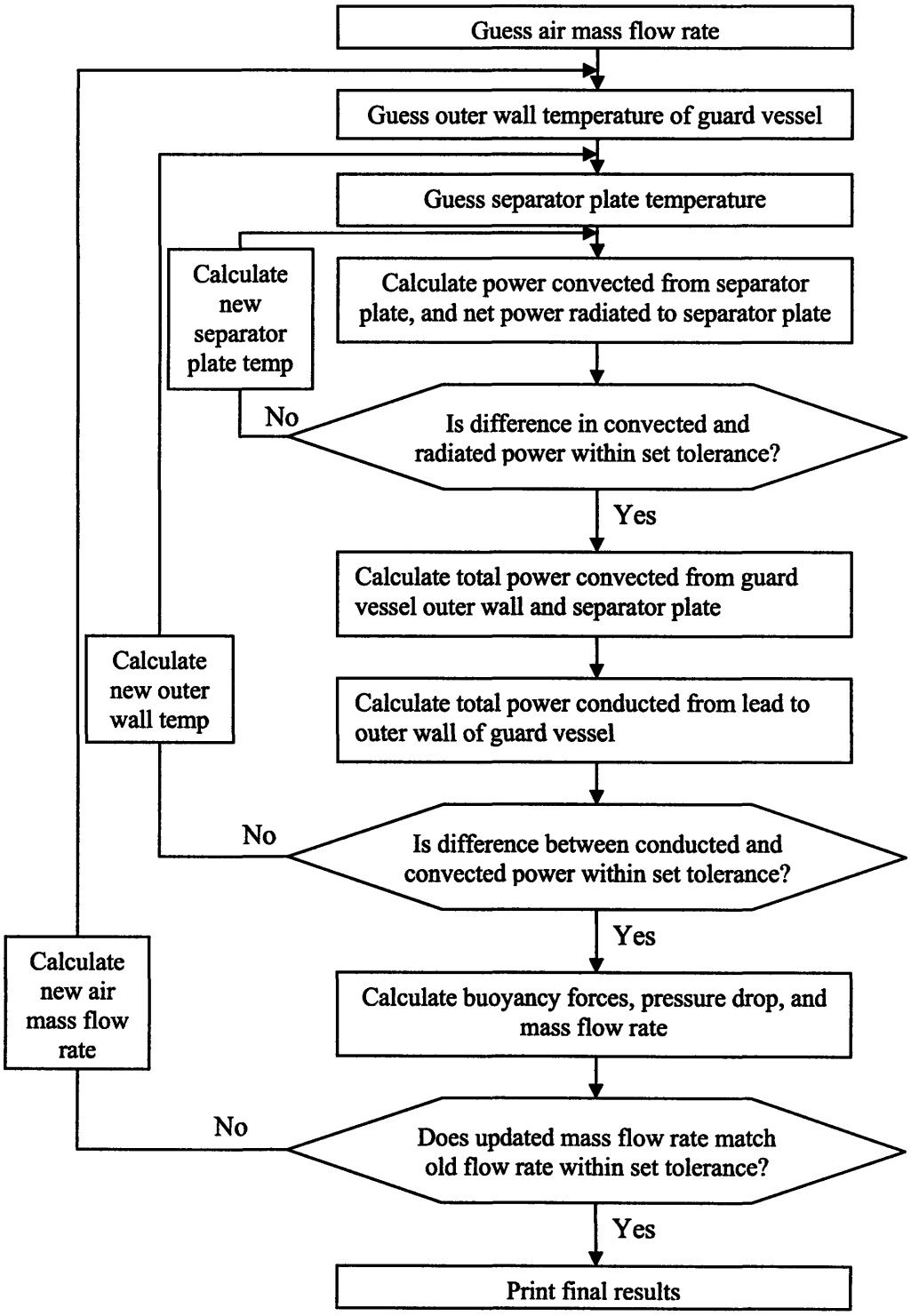

Fig. A.4. Simplified flow chart of program structure.

Energy Balances:

In order to find the temperatures of the surfaces participating in heat transfer, and the total heat transfer rate, additional energy pathways need to be considered. These different pathways are graphically described in Fig. A.5. Fin geometry depictions and naming conventions used are show in Figures A.6 and A.7.

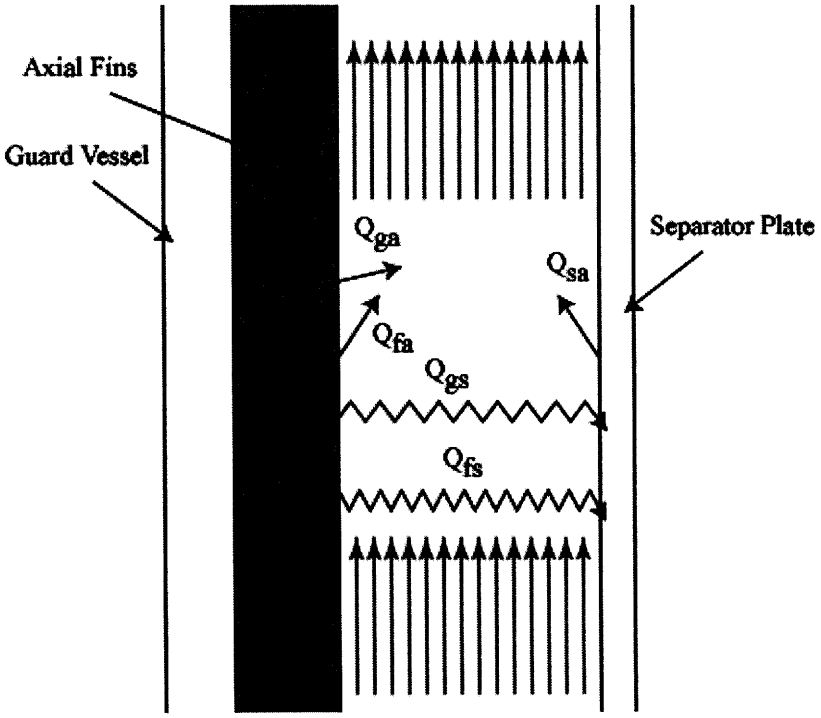

Figure A.5. Heat transfer pathways to hot air riser. Subscripts refer to guard vessel outer wall (g), axial fins (f), separator plate (s), and air (a).

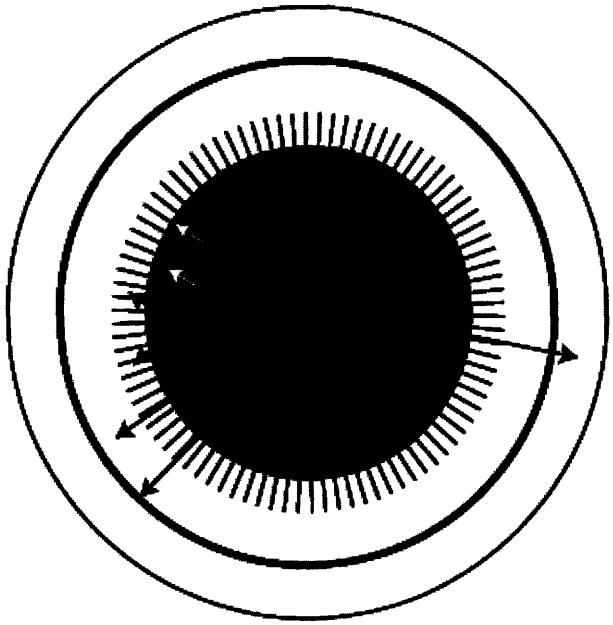

Figure A.6. Overhead view of RVACS geometry, with added fins.

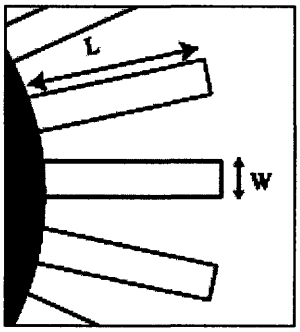

Figure A.7. Close up of fin geometry and naming conventions.

In order to model the effect of the fins on the total heat transfer, we must modify many of the energy balance equations in the bare RVACS model. First, redefine the surface area of the guard vessel as:

$$A_{guard} = (2\pi R_4 - N_{fin} W_{fin})\Delta x, \tag{A.22}$$

and the surface area of the fin tips as:

$$A_{fintip} = N_{fin} W_{fin} \Delta x, \tag{A.23}$$

where R_4 is the outer radius of the guard vessel, as shown in Fig. A.2, N_{fin} is the number of axial fins attached to the vessel, W_{fin} is the fin thickness, as shown in Fig. A.7, and Δx is the nodal length, as depicted in Fig. A.2.

Next, the heat transfer due to radiation must be modified to take into account the reduced surface area of the guard vessel, the reduced view factor between the guard vessel and the separator plate, and the radiation heat transfer between the fin tips and the separator. In order to do this, the heat transfer into the separator plate is calculated as:

$$\dot{Q}_{in,separator,j} = C_{guard} A_{guard} (T^4_{guard,j} - T^4_{separator,j}) + C_{fintip} A_{fintip} (T^4_{fintip,j} - T^4_{separator,j}), \qquad (A.24)$$

where $T_{guard,j}$, $T_{fintip,j}$, and $T_{separator,j}$ are the temperatures at node j of the guard wall, fin tips, and separator, and C_{guard} and C_{fintip} are defined as:

$$C_{guard} = F\sigma\left[\frac{1}{\varepsilon_{guard}} + \frac{A_{guard}}{A_{separator}}\left(\frac{1}{\varepsilon_{separator}} - 1\right)\right]^{-1}, \quad \text{and} \qquad (A.25)$$

$$C_{fintip} = \sigma\left[\frac{1}{\varepsilon_{fintip}} + \frac{A_{fintip}}{A_{separator}}\left(\frac{1}{\varepsilon_{separator}} - 1\right)\right]^{-1}, \qquad (A.26)$$

where F is the user-set radiation view factor between the guard vessel wall and the separator plate, σ is Boltzmann's constant, and ε_{guard}, ε_{fintip}, and $\varepsilon_{separator}$ are the emissivities of the guard vessel, fin tips, and separator plate. Since the view factor is not calculated explicitly, this addition to the model is used primarily for bracketing purposes.

Heat transfer away from the separator plate through convection to the air is not changed by the addition of fins, and so Eq. A.24 is set equal to Eq. A.5, and the separator temperature solved for.

In order to solve for the guard vessel outer wall temperature, the heat transfer enhancement of the fins must be taken into account. In order to do this, the heat transfer to the air from the fins is calculated as [Incropera and DeWitt, 2002]:

$$\dot{Q}_{out,\,fin,j} = N_{fin}\left[M\frac{\sinh(mL)+(h_j/mk)\cosh(mL)}{\cosh mL+(h_j/mk)\sinh(mL)}\right], \tag{A.27}$$

where L is the length of the fins, k is the conductivity of the fins, and M and m are defined as:

$$M = (T_{guard,j} - T_{bulkair,j})\sqrt{h_j PkA_c} = (T_{guard,j} - T_{bulkair,j})\Delta x\sqrt{2\,h_j\,k\,W_{fin}}, \tag{A.28}$$

and

$$m = \sqrt{\frac{h_j P}{k\,A_c}} = \sqrt{\frac{2\,h_j}{k\,W_{fin}}}. \tag{A.29}$$

where all values are as previously defined.

In order to calculate the guard vessel temperature, Eq. A.11 is set equal to the sum of Eqs. A.7 and A.27, where Eq. A.7 is calculated using the guard vessel nodal surface area from Eq. A.22.

The remainder of the calculations and solution follow exactly the formulae and approach as the bare-walled design.

Modification for Dimpled Wall Heat Transfer Approximation:

Modification of the code in order to approximate the effect of dimpled channel walls on heat removal is a relatively trivial process. The only modifications needed were to the convection heat transfer coefficient subroutine and the friction factor subroutine. These

factors are calculated as normal, but then multiplied by a constant coefficient, depending on what Nusselt number and friction factor augmentations are being modeled.

Modification for Perforated Plate Heat Transfer Calculation:

In order to calculate the radiant heat transfer to the perforated plate, a different set of energy balances was used, similar to but expanding upon those used for the bare walled case. The different pathways for heat from the guard vessel to the air are depicted in Fig. A.8.

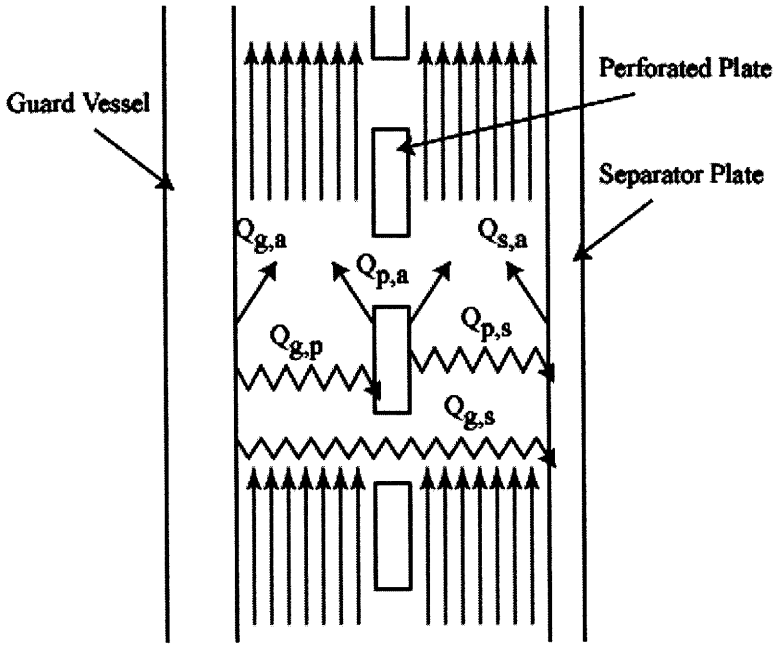

Figure A.8. Heat transfer pathways in the hot air riser. Subscripts refer to guard (g), perforated plate (p), and separator plate (s).

Three heat balances must be used to calculate temperatures and heat transfer rates from the three surfaces in the riser. They are:

$$\dot{Q}_{g,s} + \dot{Q}_{p,s} = \dot{Q}_{s,a} \ , \tag{A.30}$$

$$\dot{Q}_{g,p} = \dot{Q}_{p,s} + \dot{Q}_{p,a} \ , \tag{A.31}$$

$$\dot{Q}_{in} = \dot{Q}_{g,p} + \dot{Q}_{g,s} + \dot{Q}_{g,a} \ , \tag{A.32}$$

for the separator plate, perforated plate, and guard vessel, respectively, and where Q_{in} is the energy conducted through the guard vessel to the outer surface, calculated as in equation A.11. The radiative heat transfers, $Q_{g,s}$, $Q_{g,p}$, and $Q_{p,s}$, all can be represented by:

$$\dot{Q}_{radiation,j} = C_i A_{hot} (T_{hot,j}^4 - T_{cold,j}^4)) \ , \tag{A.33}$$

where A_{hot} is the area of the hot surface, T_{hot} and T_{cold} are the temperatures, in Kelvin, of the hot and cold surfaces, and C_i is:

$$C_i = \sigma \left[\frac{1}{\varepsilon_{hot}} + \frac{A_{hot}}{A_{cold}} \left(\frac{1}{\varepsilon_{cold}} - 1 \right) \right]^{-1} \ , \tag{A.34}$$

where σ is the Stefan-Boltzmann constant, ε_{hot} and ε_{cold} are the emissivities of the hot and cold surfaces, and A_{hot} and A_{cold} are the areas of the hot and cold surfaces. In order to accommodate the shielding effect of the perforated plate during radiation transfer between the guard vessel and the separator plate, the A_{cold} used is the area taken up by the perforations in the perforated plate.

$Q_{p,a}$, $Q_{g,a}$, and $Q_{s,a}$ are all calculated from:

$$\dot{Q}_{out,convection,j} = h_j \, A_j (T_{hot,j} - T_{bulkair,j}) , \tag{A.35}$$

where h_j is calculated from Eq. A.6, A is the heat transfer area, and $T_{hot,j}$ and $T_{bulkair,j}$ are the wall or plate temperature and the bulk air temperature at node j, respectively.

Solution Approach:

The solution approach is similar to that used in the finned vessel case, differing only in how the heat balances are calculated. In order to determine the temperature of the guard vessel outer wall, perforated plate, and separator plate, the program creates equation objects that represent the above heat balances (Eqs. A.30, A.31, and A.32). The program then iterates in order to determine the correct heat transfer within the node. The process is the same as that in the finned vessel model, except for the addition of a loop to determine separator plate temperature. The nodal energy balance section of the code is described by Fig. A.9.

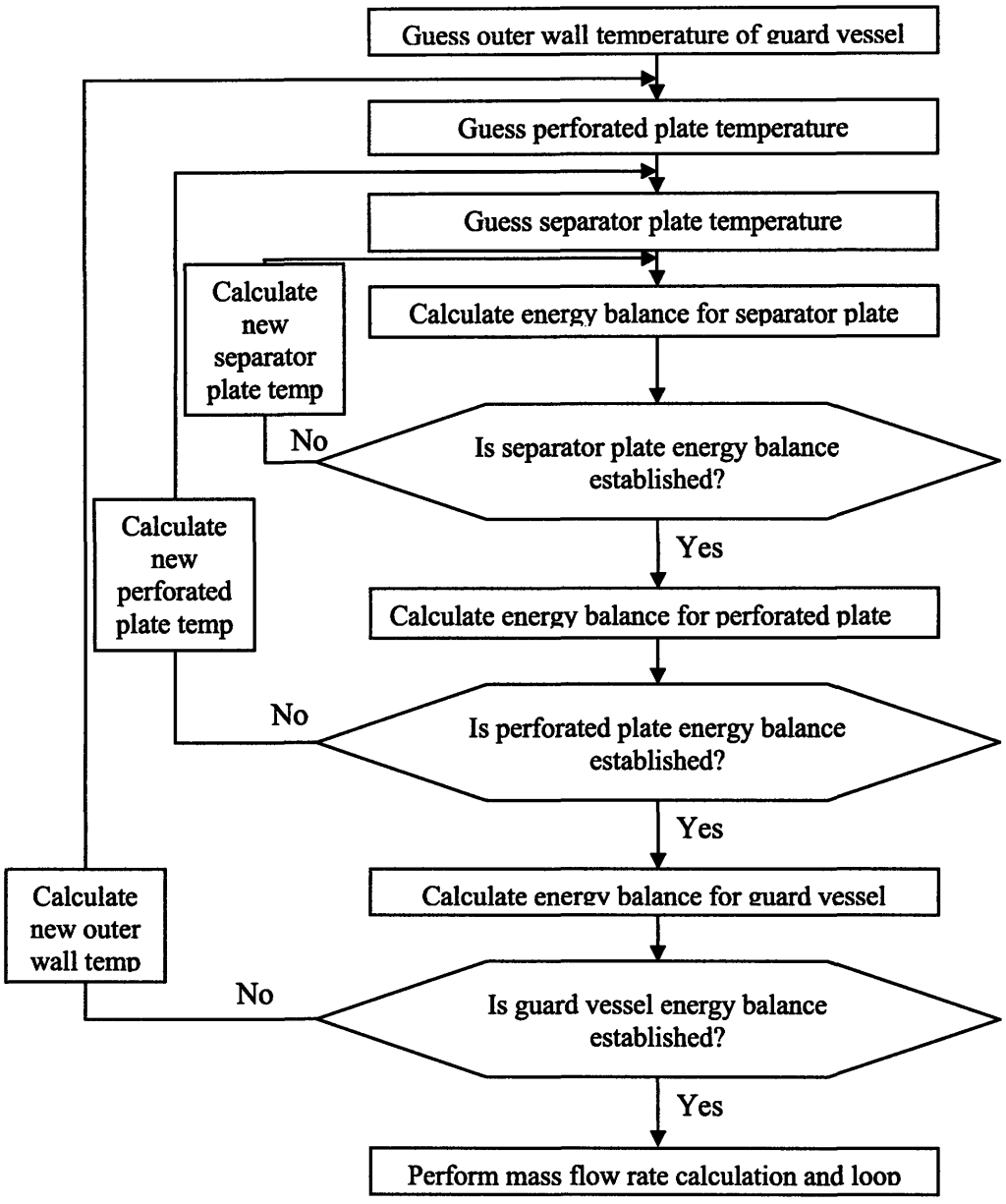

Figure A.9. Simplified flow chart of heat-balance calculations for perforated plate model.

References for Appendix A:

Heineman, J., M. Kraimer, P. Lottes, D. Pedersen, R. Stewart and J. Tessier, "Experimental and Analytical Studies of a Passive Shutdown Heat Removal System for Advanced LMRs," Proceedings of International Topical Meeting on Safety of Next Generation Power Reactors, Seattle, May, 1991

Hejzlar P., "Conceptual Design of a Large, Passive, Pressure-Tube Light Water Reactor," Doctoral Thesis, MIT, 1994.

Idel'chik, I. E., Handbook of Hydraulic Resistance, Hemisphere Pub., 2nd ed., 1986.

Incropera F., and DeWitt D., Fundamentals of Heat and Mass Transfer, Fifth Edition, John Wiley and Sons, 2002.

Irvin, T. F., Steam and Gas Tables with Computer Equations, Academic Press, New York, 1984.

White F., "Fluid Mechanics," Fifth Edition, McGraw Hill, Boston, MA, 2003.

Appendix B: Seismic analysis

Analysis of the guard vessel's ability to withstand a seismic event was performed in accordance to the analysis provided in Buongiorno and Hawkes [2004]. The approach used the Design Response Spectrum, or DRS, with a finite element analysis code to predict the peak stress imparted on a reactor vessel during an earthquake of magnitude 0.5g. A non-dimensionalization process was then performed in order to provide a quick estimate for a reactor vessel with arbitrary properties. This second approach was used in the calculation of seismic stresses for the FCR vessel.

The non-dimensionalized method used in the paper looked at the different modes of oscillation seen in the vessel and determined that the primary contributor to vessel stress was the first mode of oscillation, a simple lateral bending. Using this knowledge the differential equation for the harmonic motion of a beam with arbitrary bending moment I, mass per unit length m, Young's modulus E, and length L was solved, yielding the relation

$$f \propto \frac{1}{L^2}\sqrt{\frac{EI}{m}} \quad , \tag{B.1}$$

where f is the frequency of the first mode of oscillation.

Next, the corresponding values for the reactor vessel were plugged into this relation. L is the height of the vessel, and E is the Young's modulus of the vessel material, since the primary coolant is assumed to contribute negligibly to the rigidity of the vessel. The mass of the reactor was estimated to be equal to the mass of the primary coolant contained within, which is a good estimate for reactors with heavy-metal coolant such as the lead-cooled FCR. This yields

$$m \approx \rho\pi(r_{in}^2) \quad , \tag{B.2}$$

where m is mass per unit length, ρ is the coolant density, and r_{in} is the inner radius of the reactor vessel. Finally, the bending moment is calculated as:

$$I = \frac{\pi}{4}\left(r_{out}^4 - r_{in}^4\right) \quad , \tag{B.3}$$

where r_{out} is the outer radius of the vessel, and r_{in} is the inner radius. Note that this is a correction of a typo in the published paper.

From these relations equation B.1 becomes:

$$f \propto \sqrt{\frac{E\left(r_{out}^4 - r_{in}^4\right)}{L^4 \rho r_{in}^2}}\ , \tag{B.4}$$

and thus the dimensionless group Bu_f, assumed to be a constant, is defined as:

$$Bu_f = \frac{f}{\sqrt{\frac{E\left(r_{out}^4 - r_{in}^4\right)}{L^4 \rho r_{in}^2}}}\ . \tag{B.5}$$

From this equation the known frequency of the first mode of oscillation, calculated using the finite element analysis, was input along with vessel properties, and an average value for Bu_f was found to be 0.14 . By using this value of Buf, along with the known values for a vessel of arbitrary dimensions, material, and coolant, one can use equation B.5 to solve for the frequency of the first mode of oscillation for any vessel.

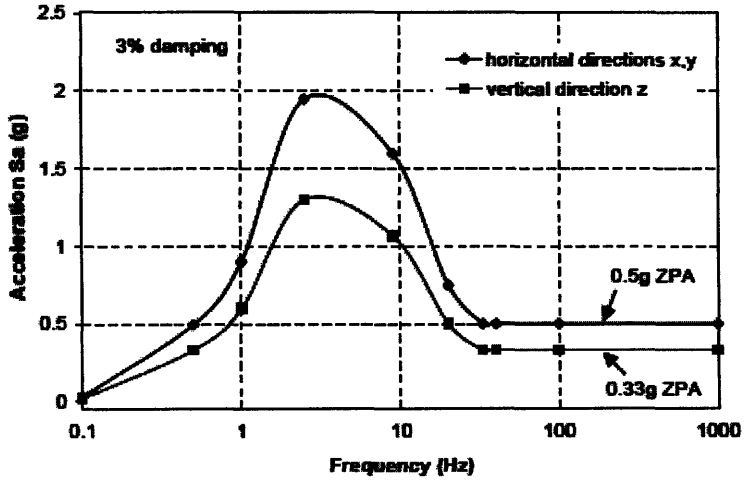

Figure B.1. The Design Response Spectrum. From Buongiorno and Hawkes [2004].

After finding the frequency, the design response spectrum, shown in Figure B.1, is used to calculate the peak acceleration, Sa. The maximum displacement, S_d of the 1st mode is given by:

$$S_d = \frac{S_a}{(2\pi f)^2}\ , \tag{B.6}$$

where f is calculated using Bu_f, and S_a is taken from the corresponding frequency on the DRS. The peak stress intensity, $S_{I,max}$, occurs at the top of the vessel, and is shown in the paper to be represented by:

$$S_{I,\max} \propto \frac{S_d E r_{out}}{L^2}\ , \tag{B.7}$$

where all variables retain their values as defined above. Equations B.4 and B.6 are plugged into equation B.7 to find:

$$S_{I,\max} \propto \frac{S_a r_{out} L^2 \rho r_{in}^2}{\left(r_{out}^4 - r_{in}^4\right)}\ , \tag{B.8}$$

which can then be used to define Bu_s as:

$$Bu_s \propto \frac{S_{I,\max}\left(r_{out}^4 - r_{in}^4\right)}{S_a r_{out} L^2 \rho r_{in}^2}\ . \tag{B.9}$$

Note that equations B.8 and B.9 both have typos in the original text. Bu_s was also averaged across the known dataset and averaged to find a value of 7.9.

By using this analysis, the maximum stress intensity of a heavy-metal filled reactor vessel can be calculated. First, the frequency of the first mode can be calculated using Eq B.5. By finding the corresponding acceleration on the DRS, the maximum stress intensity can be found using Eq. B.9. This peak stress intensity can then be compared to ASME code to assess whether it exceeds code limits.

References for Appendix B:

Buongiorno J. and Hawkes B.D., "Seismic Analysis of Heavy-Liquid-Metal-Cooled reactor vessels," Nuclear Engineering and Design, 228, pp. 305-317, 2004.